https://doi.org/10.5194/egusphere-2024-3044
Preprint. Discussion started: 30 October 2024

Exploring Atmospheric Nitrate Formation Mechanisms during the Winters of 2013 and 2018 in the North China Region via Modeling and Isotopic Analysis

Zhenze Liu[1,2], Jianhua Qi[1,2], Yuanzhe Ni[1], Likun Xue[3], Xiaohuan Liu[1,2]

[1] Key Laboratory of Marine Environment and Ecology, Ministry of Education, Ocean University of China, Qingdao 266100, China

[2] Laboratory for Marine Ecology and Environmental Science, Qingdao Marine Science and Technology Center, Qingdao 266237, China

[3] Environment Research Institute, Shandong University, Qingdao, Shandong, 266237, China

Correspondence to: Jianhua Qi (qjianhua@ouc.edu.cn), Xiaohuan Liu (liuxh1983@ouc.edu.cn)

Abstract.

Nitrate (NO_3^-) has surpassed sulfate as the dominant secondary inorganic ion, posing a significant challenge to air quality improvement in China. We utilized the WRF-CMAQ model and isotopic analysis to investigate nitrate formation mechanisms in inland and coastal cities in North China during the winters of 2013 and 2018. Among the seven nitrate formation pathways, the oxidation reaction of OH radicals with NO_2 (OH + NO_2) and the heterogeneous reaction of N_2O_5 (hetN_2O_5) were dominant pathways (88%-95.5% NO_3^-), while others contributed less than 12.4%. In inland cities, 63.7%-85.6% of nitrate formed via OH + NO_2, and 8.3%-27.7% from hetN_2O_5. In coastal cities, about half of nitrate (48.2%-56.5%) was produced from OH + NO_2, while hetN_2O_5 contributed 37.0%-45.7% due to higher N_2O_5 concentrations and longer NO_3 radical lifetimes. Compared with 2013, the OH + NO_2 contribution in 2018 increased by 7.6% in inland cities and 3.6% in coastal cities, driven by greater atmospheric oxidizing capacity. Scenario simulations showed that a 60% reduction in NO_x emissions could lower nitrate levels by 38.4%, while combined reductions in NH_3, NO_x, and VOCs led to a 59.8% decrease, from 14.6 μg/m³ to 5.9 μg/m³. These results highlight the need for comprehensive strategies targeting NH_3, NO_x, and VOCs to reduce nitrate pollution.

1 Introduction

As a key component of fine particulate matter ($PM_{2.5}$), nitrate (NO_3^-) exacerbates health risks, such as respiratory and cardiovascular diseases and premature death (Tie et al., 2009; Sun et al., 2014). Nitrate

https://doi.org/10.5194/egusphere-2024-3044
Preprint. Discussion started: 30 October 2024

substantially affects the physical and chemical properties of particulates, such as their hygroscopicity, light absorption, and acidity (Cao et al., 2013; Wang et al., 2023). These properties directly influence the atmospheric radiation balance (Ramanathan and Feng, 2009; Tegen et al., 2000), atmospheric visibility and air quality. Furthermore, nitrate serves as a key source of cloud condensation nuclei, affecting cloud formation and precipitation patterns, which subsequently influence the global water cycle and climate regulation (Yu et al., 2020; Kalkavouras et al., 2019). Moreover, the photolysis process of nitrate in atmospheric boundary layers is highly active, serving as an important source of NOx and regulating the atmospheric oxidation capacity, thus influencing the formation of secondary pollutants such as sulfate (SO_4^{2-}) and brown carbon (BrC) (Ye et al., 2016; Xue et al., 2019; Zheng et al., 2020; Yang et al., 2021). Therefore, nitrate is closely related to regional haze pollution occurrence (Zhai et al., 2021; Zhang et al., 2021; Xu et al., 2019a; Fu et al., 2020; Xu et al., 2019b). Understanding the formation mechanism of nitrate is essential not only for advancing the atmospheric chemical processes but also for providing scientific evidence to develop effective strategies for mitigating regional haze pollution.

In tropospheric atmospheres, nitrate formation primarily follows two pathways (Figure 1). During the daytime, NO_2 is oxidized by hydroxyl radicals (OH) to produce gaseous HNO_3 (R1). Conversely, at night, O_3 oxidizes NO_2, leading to the formation of the NO_3 radical, which combines with NO_2 to form N_2O_5. This compound can subsequently be absorbed onto particles via heterogeneous reactions, resulting in the formation of HNO_3 (R2) (Hallquist et al., 1999; Pathak et al., 2011). These dynamics highlight the intrinsic dependence of atmospheric nitrate formation on NO*x* and oxidants, notably O_3 and OH radicals. The generation of OH and O_3 is intricately linked to the photochemical reactions of NO*x* and volatile organic compounds (VOCs) (Atkinson, 2000). OH radicals and hydroperoxyl radicals (HO_2) are produced via the photolysis of ozone (O_3), nitrous acid (HONO), oxygenated volatile organic compounds (OVOCs), and hydrogen peroxide (H_2O_2), as well as via reactions between O_3 and VOCs. Subsequently, OH reacts with VOCs to generate organic peroxy radicals (RO_2) and HO_2, which then recycle back to OH via their interaction with nitrogen monoxide (NO). During this cycle, NO is transformed into NO_2, which, upon photolysis, yields O_3 (Fu et al., 2020).

https://doi.org/10.5194/egusphere-2024-3044
Preprint. Discussion started: 30 October 2024

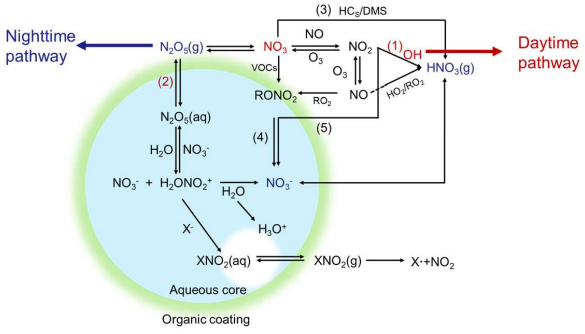

Figure 1 Formation mechanisms of nitrate in the atmosphere (Wang et al., 2023)

Nitrate formation mechanisms exhibit significant regional differences, especially in winter. For example, coastal areas, which are influenced by high humidities, high sea salt levels and the combined effect of marine emissions and air masses (Zhong et al., 2023; Athanasopoulou et al., 2008; Zhao et al., 2024), often exhibit nitrate formation mechanisms that are distinct from those in inland regions. In Beijing, which is an inland city, the contribution of the OH pathway to winter nitrate formation is 66–92%, whereas the contribution of the heterogeneous reaction of the N_2O_5 ($hetN_2O_5$) pathway ranges from 8–34% (Chen et al., 2020). In Xi'an, which is situated in the Guanzhong Basin, the contribution of the $hetN_2O_5$ pathway to winter nitrate formation ranges from 13% to 35% (Wu et al., 2021). In coastal cities in China, the contribution of the OH pathway is greater than that in inland cities, whereas the $hetN_2O_5$ pathway plays a more significant role. In Shanghai, the contribution of the OH + NO_2 pathway to winter nitrate formation is 48–74% (He et al., 2020). In Xiamen, the contributions of the OH, $hetN_2O_5$, and NO_3 + HC pathways to winter nitrate formation is 20.2%, 38.2%, and 21.6%, respectively (Li et al., 2022). Broader coastal studies have revealed similar significant regional differences. Michalski et al. (2003) noted that in coastal California, approximately 90% of winter nitrate originates from the $hetN_2O_5$ pathway. Kunasek et al. (2008) reported that in the polar environment of Greenland, nearly all nitrate is formed via the NO_3 + HC/DMS and $hetN_2O_5$ pathways in winter, with contributions of 60% and 40%, respectively. Furthermore, the impacts of continental and marine air masses on nitrate formation mechanisms differ. In the South Yellow Sea, under the dominance of marine air masses, the contributions of the OH + NO_2, NO_3 + HC/DMS, and $hetN_2O_5$ pathways to nitrate formation are 43.9%, 22.4%, and 33.6%, respectively, while the contributions (12.6%, 59.0%, and 28.4%, respectively) in the Bohai and North Yellow Seas are affected by continental pollution (Zhao et al., 2024). These studies have confirmed substantial regional differences in nitrate formation mechanisms. However, present research remains

https://doi.org/10.5194/egusphere-2024-3044
Preprint. Discussion started: 30 October 2024

confined to individual regions, and a thorough land–ocean comparison analysis is lacking. Additionally, the environmental factors and interactions driving these differences have not been systematically explored, leading to a limited understanding of the regional differences in nitrate formation mechanisms. The North China Plain (NCP) region is a focal point because of regional winter haze issues, which consistently ranks among the areas with the highest concentrations of $PM_{2.5}$ globally (Chen et al., 2016). Before 2013, sulfate was the primary pollutant during haze events in the NCP, comprising a significant proportion of $PM_{2.5}$ (Li et al., 2019). In 2013, the Clean Air Action Plan (CAAP) was initiated in China to reduce $PM_{2.5}$ concentrations and promote air quality improvement (Air Pollution Prevention and Control Action Plan, 2013). Following the initiation of this clean air campaign, winter haze pollution shifted from being dominated by sulfate to being dominated by nitrate (Li et al., 2019; Xu et al., 2019a). According to data from the Multiresolution Emission Inventory for China (MEIC) (Zheng et al., 2018) from 2013 to 2017, anthropogenic SO_2, NOx, CO, and NH_3 emissions decreased by 59%, 21%, 23%, and -3%, respectively. Correspondingly, the national annual average $PM_{2.5}$ level decreased by 30–50% from 2013–2018 (Zhai et al., 2019). Therefore, emission reduction measures led to a substantial decrease in the CO and SO_2 levels, as well as a reduction in particulate sulfate concentrations. However, the reduction in particulate nitrate levels was smaller than anticipated. In major cities, the mass concentration of nitrate has even increased (Xu et al., 2019b; Shao et al., 2018; Zhou et al., 2019; Fu et al., 2020). The difference in these changes between nitrate and sulfate highlights the complex relationship between nitrate and its precursors, emphasizing the importance of fully understanding nitrate chemistry in particulate matter.

Currently, most studies have focused on nitrate formation mechanisms in inland cities (Fan et al., 2020b; Fu et al., 2020; Yang et al., 2024; Chen et al., 2020), but the formation mechanisms in coastal cities remain poorly understood. Therefore, it is necessary to compare nitrate formation mechanisms between inland and coastal cities, especially during periods dominated by different primary pollutants. To address this issue, we selected the winters of 2013, when the CAAP was initiated, and 2018, after the plan had concluded, to explore the nitrate formation mechanisms in five inland cities and two coastal cities on the NCP. This approach allowed us to better understand the evolution of major nitrate aerosol formation mechanisms before and after the implementation of emission control measures in inland and coastal regions. Overall, these results increase our understanding of the role of nitrate formation mechanisms in

https://doi.org/10.5194/egusphere-2024-3044
Preprint. Discussion started: 30 October 2024

atmospheric chemistry.

2 Methods

2.1 Model configuration

The Community Multiscale Air Quality (CMAQ) model (version 5.3.3) was used to simulate the chemical reactions and physical processes that contribute to NO_3^- and TNO_3 ($HNO_3 + NO_3^-$) formation in the NCP region. Two distinct periods were considered, i.e., one period from December 1, 2013, to February 28, 2014, representing the period when the CAAP was initiated, and one period from December 1, 2018, to February 28, 2019, representing the period after the CAAP was completed. As shown in Figure 2, a dual-layer grid nesting method was implemented in our simulations. Domain 1 (D01) encompasses the majority of China with a 36-km horizontal resolution, whereas domain 2 (D02) covers the NCP with a 12-km horizontal resolution. The major cities within the NCP include Beijing (BJ), Tianjin (TJ), Shijiazhuang (SJZ), Jinan (JN), Zhengzhou (ZZ), Qingdao (QD), and Yantai (YT). The model was vertically segmented into 14 layers, stretching from the Earth's surface up to the troposphere, with the first layer height at approximately 31 m. The CB6 chemical mechanism was chosen to simulate gas-phase chemistry (Luecken et al., 2019; Yan et al., 2021) and the aerosol mechanism. Aerosol module version 7 (AERO7, Appel et al. 2020) was used to simulate particulate-phase chemistry. The initial and boundary conditions used as the inputs of D01 were provided via the GEOS-Chem global simulation results, and D02 was provided via D01. To minimize the impact of the initial conditions, we initiated the model run 7 days before the analysis period. Anthropogenic emission data were sourced from the MEIC source emission inventory maintained by Tsinghua University (http://meicmodel.org/), while biogenic emission estimates were derived from the Model of Emissions of Gases and Aerosols from Nature version 2.0.4 (MEGANv2.0.4, http://lar.wsu.edu/megan/).

https://doi.org/10.5194/egusphere-2024-3044
Preprint. Discussion started: 30 October 2024

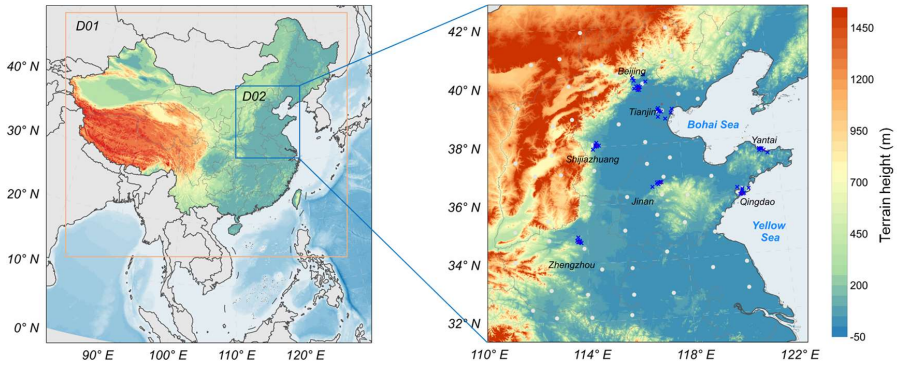

Figure 2 Terrain heights of the NCP region and locations of the major cities (Beijing, Tianjin, Shijiazhuang, Jinan, Zhengzhou, Qingdao, and Yantai) within the study domain. The white dots indicate meteorological observation stations, and the blue crosses indicate air quality monitoring stations.

The required meteorological data were generated with the Weather Research and Forecasting Model (WRF) version 3.7, a system for predicting mesoscale weather patterns. The selection of physics options for this model conforms with the methodologies applied in our earlier studies (Liu et al., 2021; Chen et al., 2021). The WRF simulations in this study depend on the Final Operational Global Analysis (FNL) datasets, which are global reanalysis data with temporal and spatial resolutions of 6 hours and 1°×1°, respectively, provided by the U.S. Environmental Prediction Center and the National Center for Atmospheric Research (https://rda.ucar.edu/datasets/ds083-2/). The WRF model outputs were subsequently processed via Model-3/CMAQ Modeling System Interface Processor (MCIP) version 4.3, ensuring compatibility with the CMAQ model format.

2.2 Process analysis

Within the CMAQ modeling framework, the Integrated Reaction Rate (IRR) module of the Process Analysis (PA) tool was used to simulate the formation reactions of TNO_3 ($HNO_3 + NO_3^-$). The reaction rates of the chemical reactions at each moment were provided by the IRR module, enabling the quantitative evaluation of the target reactions. The complex chemical formation of TNO_3 involves seven reaction pathways, which are categorized into three main pathways on the basis of their significance, i.e., $OH + NO_2$ (R1), hetN_2O_5 (R2), and other formation pathways (R3 + R4 + R5 + R6 + R7). The chemical equations for these seven production reaction pathways are as follows:

$$NO_2(g) + OH(g) \rightarrow HNO_3(g) \quad \text{(R1)}$$

$$N_2O_5 + H_2O(l) \rightarrow 2HNO_3(aq) \quad \text{(R2)}$$

$$N_2O_5(g) + H_2O(g) \rightarrow 2HNO_3(g) \quad \text{(R3)}$$

https://doi.org/10.5194/egusphere-2024-3044
Preprint. Discussion started: 30 October 2024

$NO_3(g) + VOCs(g) \rightarrow HNO_3(g)$ (R4)

$2NO_2(g) + 2H_2O(l) \rightarrow HNO_3(aq) + HONO(aq)$ (R5)

$ClNO_3(g) + H_2O(l) \rightarrow HNO_3(aq) + HOCl(aq)$ (R6)

$RONO_2(g) + H_2O(l) \rightarrow HNO_3(aq) + ROH(l)$ (R7)

2.3 Observation data

In this study, the simulation results, including meteorological parameters and atmospheric pollutants, for the major cities in the NCP were validated in depth. The meteorological parameters included the 2-m temperature (T2), relative humidity (RH), 10-m wind speed (WS10), and 10-m wind direction (WD10). Atmospheric pollutants included the maximum 8-hour moving average ozone ($MDA8O_3$), NO_2, $PM_{2.5}$, and $PM_{2.5}$ components.

2.3.1 Meteorological data and sources

Meteorological data, comprising T2, WS10, WD10, and RH, were sourced from the National Climatic Data Center (NCDC) of the National Oceanic and Atmospheric Administration (NOAA) (https://www.ncdc.noaa.gov/cdo-web/, last access: 17 October 2023). Data were collected from a total of 68 stations, with a temporal resolution of either 3 hours or 1 hour.

2.3.2 Atmospheric pollutant concentrations

Data of O_3, NO_2, and $PM_{2.5}$ concentrations were retrieved from the real-time national urban air quality dataset disseminated by the China Environmental Monitoring Center (https://air.cnemc.cn:18007/). Data of SO_4^{2-}, NH_4^+ and NO_3- concentrations were sourced from our own observations in Qingdao and published data (detailed information can be found in Table S3).

In Qingdao city, we collected total suspended particle (TSP) samples during two winter seasons. The TSP samples were collected on preheated quartz fiber filters with a high-volume (1.05 m^3 min^{-1}) aerosol sampler (Qingdao Laoshan Electronics Co., Ltd., China). The sampling site was situated on the roof of Darwin Hall (36°06′N, 120°33′E, 16 m) at Ocean University of China, approximately 1 km away from the beach. Detailed information can be found in Ding et al. (2019). Water-soluble inorganic ions, such as NO_3^-, SO_4^{2-}, and NH_4^+, were extracted with ultrapure water (> 18.2 MΩ·cm) via a Thermo Scientific Dionex ICS-1100 IC system, as reported in a previous study (Qi et al., 2020). The ionic concentrations in the TSP samples were calibrated by subtracting the concentrations in the blanks. The $\delta^{18}O$ and $\delta^{15}N$

https://doi.org/10.5194/egusphere-2024-3044
Preprint. Discussion started: 30 October 2024

values of NO_3^- in the TSP samples were determined via the denitrifier method (Casciotti et al., 2002; Sigman et al., 2001). For analytical calibration, four international reference standards were employed, namely, USGS32, USGS34, USGS35, and IAEA-NO_3^-. The standard deviations of the replicates were ±0.2‰ for $\delta^{15}N\text{-}NO_3^-$ and ±0.5‰ for $\delta^{18}O\text{-}NO_3^-$. The analytical procedures for determining $\delta^{15}N\text{-}NO_3^-$ and $\delta^{18}O\text{-}NO_3^-$ have been detailed in a previous study (Luo et al., 2021).

2.4 Dual-isotopic Bayesian mixing model

The Bayesian isotope mixing model (Stable Isotope Analysis in R, SIAR) and dual-isotopic compositions ($\delta^{15}N\text{-}NO_3^-$ and $\delta^{18}O\text{-}NO_3^-$) determined in Qingdao and adapted from a reference study in Beijing (Zong et al., 2020; Fan et al., 2020b) were employed to estimate the contributions of OH radicals and the hetN_2O_5 pathway to particulate NO_3^-. Eqs. (S1) to (S7) for calculating the isotopic compositions of nitrogen oxides in the atmosphere are provided in the Supporting Information. The atmospheric $\delta^{15}N\text{-}NO_3^-$ and $\delta^{18}O\text{-}NO_3^-$ can be expressed by Eqs. (S1) and (S2), respectively. The end-members of $[\delta^{15}N\text{-}HNO_3]_{OH}$, $[\delta^{15}N\text{-}HNO_3]_{N2O5}$, $[\delta^{18}O\text{-}HNO_3]_{OH}$ and $[\delta^{18}O\text{-}HNO_3]_{N2O5}$ can be expressed by Eqs. (S3), (S4), (S5) and (S6), respectively (Walters and Michalski, 2016). The $\delta^{15}N$ values of tropospheric NOx and the $\delta^{18}O$ values of tropospheric $H_2O_{(g)}$, NOx, O_3, and OH occurred within a certain range, as described in Text S1. Therefore, the end-members of $\delta^{15}N$ and $\delta^{18}O$ for the two pathways can be estimated by f_{NO2} (the molar ratio of NO_2 and NOx) and the isotope fractionation values of nitrogen and oxygen, i.e., $\alpha_{NO2/NO}$, $\alpha_{OH/H2O}$, and $\alpha_{N2O5/NO2}$. The nitrogen and oxygen isotope fractionations are temperature dependent and can be estimated via Eq. (S7) and Table S1. On the basis of the end-members of $[\delta^{15}N\text{-}HNO_3]_{OH}$, $[\delta^{15}N\text{-}HNO_3]_{N2O5}$, $[\delta^{18}O\text{-}HNO_3]_{OH}$ and $[\delta^{18}O\text{-}HNO_3]_{N2O5}$, the contribution of the OH radical formation pathway (γ) was estimated via the dual-isotopic Bayesian mixing model (Luo et al., 2021).

2.5 Model evaluation

The following statistical indicators were used to evaluate the simulation effect: the mean deviation (MB), normalized mean deviation (NMB), normalized mean error (NME), correlation coefficient (R), root mean square error (RMSE), and index of agreement (IOA). The definitions and standards of all the statistical indicators are provided in Table S2. Emery et al. (2017) and Huang et al. (2021) proposed benchmarks for the concentrations of major air pollutants, including $PM_{2.5}$, NO_2, $MDA8O_3$, and NO_3^-. Similarly, Emery et al. (2001) provided benchmarks for major meteorological parameters such as T2, WS10 and

https://doi.org/10.5194/egusphere-2024-3044
Preprint. Discussion started: 30 October 2024

WD10.

2.6 Emission reduction scenario simulation design

Notably, emission reduction scenarios were designed to examine the effects of reducing NH_3, NOx, and VOC emissions on nitrate concentrations in $PM_{2.5}$ in the NCP region. The simulations included single-pollutant reduction strategies for NH_3, NOx, and VOCs, as well as combined reduction scenarios. For each pollutant, emissions were reduced by 20%, 40%, and 60%, with a focus on assessing the resulting influence on nitrate formation. The combined reduction scenarios entailed simultaneous reductions in NH_3, NOx, and VOCs to evaluate synergistic effects. The nitrate concentration responses to these reductions were analyzed to determine the most effective strategies for controlling winter nitrate levels.

3 Results and discussion

3.1 Model evaluation

3.1.1 Evaluation of meteorological parameters

Table 1 Statistical performance of the modeled meteorological parameters in the NCP during the winters of 2013 and 2018 (68 sites).

	Winter, 2013				Winter, 2018				Benchmark			
Parameters	MB	RMSE	IOA	R	MB	RMSE	IOA	R	MB	RMSE	IOA	R
T2/℃	0.60	3.25	0.93	0.88	1.15	3.14	0.94	0.90	≤±0.5	/	≥±0.8	/
RH/%	-3.67	17.53	0.82	0.69	-5.35	19.36	0.81	0.68	/	/	/	/
WS10/(m·s^{-1})	1.55	2.79	0.61	0.47	1.47	2.72	0.60	0.46	≤±0.5	≤±2.0	≥0.6	/
WD10/°	5.44	115.02	0.70	0.43	-1.65	121.00	0.69	0.42	≤±10	/	/	/

*** *T2* denotes the 2-m temperature, *RH* denotes the relative humidity, *WS10* denotes the 10-m wind speed, and *WD10* denotes the 10-m wind direction.**

The statistical model performance for meteorological parameters such as T2, WS10, WD10, and RH in the NCP is summarized in Table 1, covering the winter months from December 2013 to February 2014 (winter, 2013) and from December 2018 to February 2019 (winter, 2018). The simulated T2 and RH values exhibited satisfactory reproducibility, with temperature simulations exhibiting slightly higher MB values above the recommended threshold (MB≤±0.5). The simulated wind speeds during both winters were slightly overestimated, with the RMSE slightly exceeding the good model performance criterion (2 m/s; Emery et al. (2001)), whereas the wind direction results fully satisfied the criterion. The observed wind speed overestimation by the WRF model could be attributed to its inability to accurately capture the impact of high aerosol loadings on shortwave radiation in winter, which likely reduced the near-surface wind speed (Tan et al., 2017; Jacobson and Kaufman, 2006). In general, the meteorological field

https://doi.org/10.5194/egusphere-2024-3044
Preprint. Discussion started: 30 October 2024

simulations of the WRF model are reliable and can effectively reveal the changes in various meteorological elements in the NCP.

3.1.2 Evaluation of atmospheric pollutants

As indicated in Table 2, the model exhibited a favorable simulation ability for the concentrations of NO_2, $MDA8O_3$ and $PM_{2.5}$ pollutants in the NCP region. Specifically, the simulations accurately captured NO_2 concentrations, with NMB values ranging from -30% to 32%. Notably, during the winter of 2018, the simulated NO_2 concentration in Beijing was slightly higher, exceeding the acceptable range by 2%, whereas that in other cities remained within the acceptable range. The $MDA8O_3$ simulations generally exhibited slight underestimation, whereas in Tianjin, Shijiazhuang, and Zhengzhou, the simulations slightly exceeded the standard. This was primarily due to the uncertainty in anthropogenic VOC emissions (Wang et al., 2014), making accurate ozone simulations particularly challenging (Sun et al., 2022; Yang et al., 2024). The $PM_{2.5}$ simulations were generally accurate, although the simulated concentrations in Tianjin during the winter of 2013 were slightly elevated, with an NMB of 32%, exceeding the standard by 2%, but those in the other cities met the standard requirements.

Table 2 Model performance for the major air pollutants in typical cities of the NCP during the winters of 2013 and 2018.

City	Pollutants ($\mu g/m^3$)	2013 winter				2018 winter			
		NMB	NME	MB	R	NMB	NME	MB	R
Beijing (BJ)	MDA8 O_3	-5%	25%	-2.04	0.76	-13%	25%	-6.80	0.68
	NO_2	1%	19%	0.08	0.89	32%	46%	13.85	0.73
	$PM_{2.5}$	-16%	28%	-17.41	0.88	-10%	45%	-5.11	0.64
Tianjin (TJ)	MDA8 O_3	-4%	30%	-1.23	0.73	-29%	33%	-14.19	0.63
	NO_2	8%	22%	5.53	0.76	26%	39%	14.16	0.68
	$PM_{2.5}$	32%	41%	34.73	0.81	2%	51%	1.75	0.62
Shijiazhuang (SJZ)	MDA8 O_3	-15%	29%	-5.49	0.64	-25%	35%	-11.25	0.58
	NO_2	-5%	27%	-3.66	0.73	12%	32%	7.40	0.61
	$PM_{2.5}$	-25%	34%	-48.32	0.80	-20%	39%	-23.13	0.59
Jinan (JN)	MDA8 O_3	2%	25%	0.87	0.77	-11%	31%	-6.41	0.54
	NO_2	-14%	20%	-10.20	0.73	-8%	30%	-5.01	0.61
	$PM_{2.5}$	-7%	21%	-9.54	0.85	-10%	33%	-8.82	0.70
Zhengzhou (ZZ)	MDA8 O_3	-6%	49%	-2.65	0.03	1%	34%	0.16	0.63
	NO_2	12%	24%	7.52	0.69	11%	34%	6.10	0.61
	$PM_{2.5}$	24%	33%	30.63	0.85	-9%	36%	-10.34	0.63
Qingdao (QD)	MDA8 O_3	-1%	21%	-0.66	0.82	-3%	22%	-1.91	0.47
	NO_2	11%	23%	7.52	0.69	-4%	28%	-1.99	0.76
	$PM_{2.5}$	4%	21%	3.70	0.89	-3%	38%	-1.84	0.70
Yantai (YT)	MDA8 O_3	5%	17%	2.48	0.79	-10%	22%	-6.50	0.27
	NO_2	-30%	32%	-15.34	0.81	-9%	33%	-3.31	0.78
	$PM_{2.5}$	-6%	25%	-4.09	0.84	-19%	33%	-10.84	0.78
Benchmark	MDA8 O_3	≤±15%	< 25%	/	> 0.50	/	/	/	/
	NO_2	≤±30%	≤75%	/	/	/	/	/	/
	$PM_{2.5}$	≤±30%	< 50%	/	> 0.40	/	/	/	/

*** The benchmarks for these pollutants, including NO_2 according to Us-Epa (2007); MDA8 O_3 and $PM_{2.5}$, were proposed by Emery et al. (2017) and Huang et al. (2021).**

https://doi.org/10.5194/egusphere-2024-3044
Preprint. Discussion started: 30 October 2024

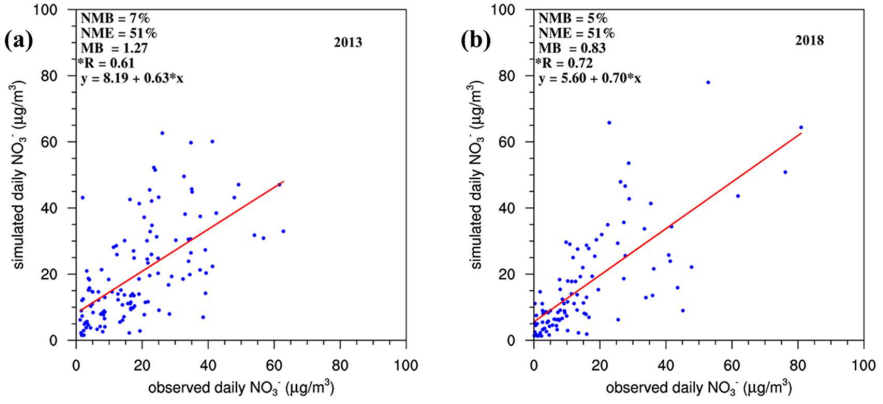

Figure 3 Scatter plots of the simulated and observed daily mean NO_3^- concentrations in the NCP during the winter seasons of 2013 and 2018; the * symbol indicates statistical significance ($P < 0.05$).

Figure 3 shows a comparison of the simulated and observed NO_3^- concentrations in the six NCP cities during the winters of 2013 and 2018. Yantai was excluded from the comparison because of insufficient observation data. The comparison results indicated that the simulated NO_3^- trends in the NCP were accurate during the winters of both 2013 and 2018, with R values of 0.61 and 0.72, respectively, meeting the established standard of 0.60. However, the simulation for 2013 yielded slightly overestimated values, with an MB of 1.27, corresponding to NMB = 7% and NME = 51%. In contrast, the simulation results for 2018 were closer to the observed values, with NMB = 5% and NME = 51%. Overall, the model demonstrated suitable stability and accuracy in simulating atmospheric pollutants in the NCP region, providing a solid foundation for future analysis.

3.2 Variations in the concentrations of $PM_{2.5}$ and its components between 2013 and 2018

During the winter of 2013, the average $PM_{2.5}$ concentration in the NCP reached 80.52 μg/m³, with high-concentration areas mainly concentrated in Beijing, Tianjin, southern Hebei, Henan, Shandong, and Anhui Provinces (Figure 4). However, the average $PM_{2.5}$ concentration in this region decreased to 50.74 μg/m³ in 2018, a significant reduction of 37% compared with that in 2013. Li et al. (2023) also reported that between 2013 and 2018, the $PM_{2.5}$ concentration in China decreased by 39.5%, with a reduction of 40.8% in the Beijing-Tianjin-Hebei region. Additionally, observation data from the China National Environmental Monitoring Center (CNEMC) showed that the annual average $PM_{2.5}$ levels in China decreased by 30% to 50% from 2013–2018 (Zhai et al., 2019). SO_4^{2-}, NO_3^- and ammonium (NH_4^+)

https://doi.org/10.5194/egusphere-2024-3044
Preprint. Discussion started: 30 October 2024

significantly affect $PM_{2.5}$ concentration changes (Peng et al., 2024; Zheng et al., 2015). We found that the SO_4^{2-} concentration decreased significantly by 53%, whereas the NO_3^- and NH_4^+ concentrations decreased by 13% and 33%, respectively (refer to Figure S1 for city-specific changes), affected by emission reduction. The observation data (Li et al., 2019; Zhang et al., 2019) also confirmed our model results, namely, SO_4^{2-} exhibited the greatest reduction, followed by NH_4^+ and NO_3^-. For example, the SO_4^{2-}, NH_4^+, and NO_3^- concentrations in Beijing decreased by 52%, 43%, and 25%, respectively, from 2013 to 2017, whereas those in Tianjin decreased by 27%, 23%, and 7%, respectively(Zhang et al., 2019). The substantial reduction in the three inorganic components, namely, SO_4^{2-}, NH_4^+, and NO_3^-, led to significant variation in the $PM_{2.5}$ composition.

The decrease in the concentration led to a significant reduction in the proportion of SO_4^{2-} in $PM_{2.5}$ but an increase in the proportion of nitrate during the winters of 2013 to 2018 (Figure 5). Specifically, the average SO_4^{2-} concentration decreased from 13.46 μg/m³ during the winter of 2013 to 6.37 μg/m³ during the winter of 2018, with its proportion in $PM_{2.5}$ decreasing from 16.7% to 12.6% (Figure 6). In contrast, although the NO_3^- concentration slightly decreased from 16.5 μg/m³ during the winter of 2013 to 14.6 μg/m³ during the winter of 2018, its proportion in $PM_{2.5}$ increased from 20.5% to 28.7%. The change in the NO_3^-/SO_4^{2-} ratio is an important indicator for assessing pollution sources and key chemical transformations in the atmosphere. Our results indicated that this ratio was 1.2 in 2013 and increased to 2.29 in 2018 in the NCP. The observation data for Beijing also demonstrated a similar variation trend, with the NO_3^-/SO_4^{2-} ratio increasing from 0.72±0.59 in 2014 to 1.36±0.90 in 2016 (Xu et al., 2019b). The variation in the NO_3^-/SO_4^{2-} ratio revealed that the main pollution components of $PM_{2.5}$ in the NCP shifted from SO_4^{2-} to NO_3^-. This finding has also been widely confirmed in recent studies (Fu et al., 2020; Wang et al., 2020b; Xie et al., 2020; Xu et al., 2019b), suggesting that NO_3^- plays an increasingly important role in $PM_{2.5}$ formation. Therefore, further research on the nitrate formation mechanism is crucial for alleviating $PM_{2.5}$ pollution in the complex chemical environments of the NCP.

https://doi.org/10.5194/egusphere-2024-3044
Preprint. Discussion started: 30 October 2024

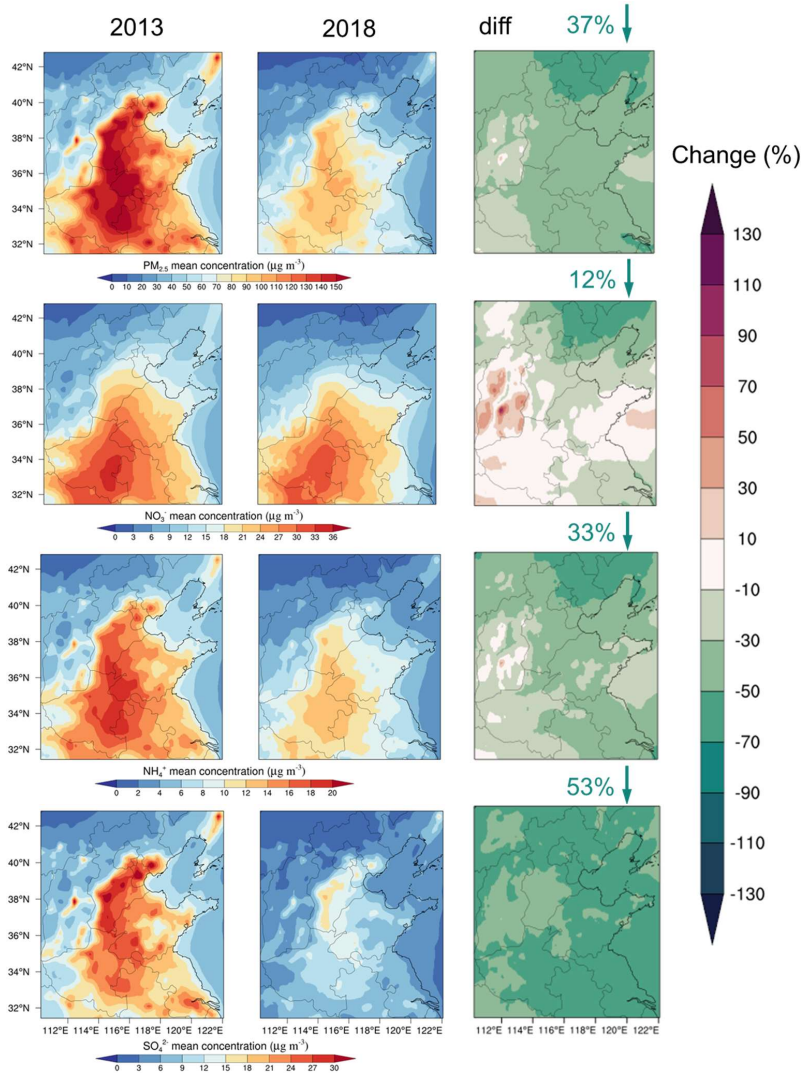

Figure 4 Spatial distribution and changes in $PM_{2.5}$ and its components in the NCP during the winters of 2013 and 2018. The up arrows indicate increases, and the down arrows indicate decreases.

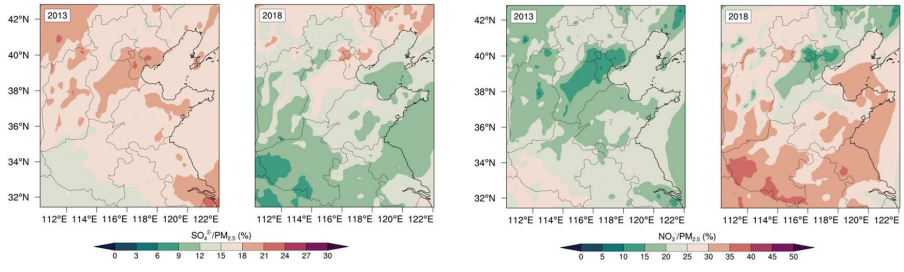

Figure 5 Spatial distributions of the nitrate and sulfate proportions in $PM_{2.5}$ in the NCP region during the winters of 2013 and 2018

https://doi.org/10.5194/egusphere-2024-3044
Preprint. Discussion started: 30 October 2024

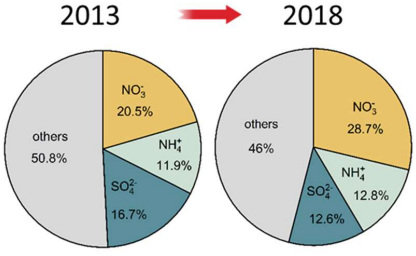

Figure 6 Changes in the proportions of the $PM_{2.5}$ components in the NCP region during the winters of 2013 and 2018

3.3 Rates, contributions and diurnal variations in nitrate formation reactions in the major cities

As mentioned above, the NO_3^- concentration slightly decreased from 2013 to 2018. We found that the decrease was due to a decrease in the TNO_3 production rate (0–0.05 ppb/h), which could be attributed to the production rate of the hetN_2O_5 pathway (0–0.03 ppb/h), as detailed in Table 3. Owing to the decreased reaction rate of the hetN_2O_5 pathway, its contribution in these seven cities was reduced by -2.1% to 7.8%. For the OH + NO_2 reaction pathway, the rate remained unchanged except in four cities (Beijing, Jinan, Zhengzhou, and Qingdao), whereas it varied between -0.02 and 0.01 ppb/h in the other cities. However, the contribution of the OH + NO_2 reaction pathway to TNO_3 formation increased overall due to the decreased rate of the hetN_2O_5 reaction pathway, although the production rate remained almost unchanged. Moreover, the contribution increase was greater in inland cities than in coastal cities. In the five inland cities (Beijing, Tianjin, Shijiazhuang, Jinan, and Zhengzhou), the OH + NO_2 reaction pathway was the main nitrate formation mechanism, with its contribution ratio ranging from 63.7%–77.8% in 2013 increasing to 72.9%–85.6% in 2018. In contrast, in the two coastal cities (Qingdao and Yantai), the OH + NO_2 reaction pathway contributed 48.2%–56.5% to nitrate formation, whereas the contribution of the hetN_2O_5 pathway ranged from 37.0%-45.7%, which indicated that both pathways were equally important in nitrate formation in the coastal cities. These findings highlighted a significant marine–land contrast in the nitrate formation mechanisms within the NCP region. The differences between the inland and coastal cities were particularly notable, demonstrating that the nitrate formation mechanisms varied substantially with geographic location.

https://doi.org/10.5194/egusphere-2024-3044
Preprint. Discussion started: 30 October 2024

Table 3 TNO_3 production rates (ppb/h) in the surface layer and contributions (%) of the major production pathways in the surface atmosphere in seven representative cities of the NCP in 2013 and 2018

City	Year	Production rates (ppb/h)			Daytime Contribution (%)			Nighttime Contribution (%)			Total Contribution (%)		
		TNO_3	$OHNO_2$	$hetN_2O_5$	$OHNO_2$	$hetN_2O_5$	Other	$OHNO_2$	$hetN_2O_5$	Others	$OHNO_2$	$hetN_2O_5$	Others
BJ	2013	0.19±0.15	0.15±0.16	0.03±0.02	90.2%	5.2%	4.6%	33.4%	46.9%	19.7%	77.8%	14.3%	7.9%
	2018	0.17±0.15	0.15±0.16	0.02±0.01	95.1%	2.6%	2.3%	48.4%	39.4%	12.2%	85.6%	9.9%	4.5%
TJ	2013	0.22±0.17	0.15±0.19	0.04±0.03	85.7%	6.5%	7.8%	15.2%	58.8%	25.9%	67.8%	19.7%	12.4%
	2018	0.17±0.15	0.13±0.17	0.03±0.02	92.2%	3.9%	3.9%	22.4%	57.1%	20.4%	77.5%	15.1%	7.4%
SJZ	2013	0.19±0.16	0.14±0.17	0.03±0.01	87.8%	5.5%	6.6%	21.2%	46.8%	32.0%	73.8%	14.2%	12.0%
	2018	0.18±0.17	0.15±0.18	0.02±0.01	93.8%	2.0%	4.2%	30.3%	41.1%	28.6%	83.6%	8.3%	8.1%
JN	2013	0.26±0.14	0.16±0.18	0.07±0.05	85.1%	8.9%	6.0%	21.1%	65.4%	13.5%	63.7%	27.7%	8.5%
	2018	0.22±0.15	0.16±0.18	0.04±0.03	90.7%	4.4%	4.9%	27.6%	59.5%	12.9%	72.9%	19.9%	7.1%
ZZ	2013	0.24±0.21	0.19±0.23	0.03±0.01	88.9%	4.7%	6.4%	26.8%	37.4%	35.8%	77.6%	10.6%	11.8%
	2018	0.24±0.20	0.19±0.22	0.03±0.02	91.9%	3.1%	5.0%	32.8%	47.5%	19.6%	79.2%	12.7%	8.2%
QD	2013	0.27±0.09	0.14±0.14	0.11±0.07	75.8%	17.8%	6.4%	16.5%	75.6%	7.9%	51.5%	41.5%	7.0%
	2018	0.25±0.09	0.14±0.15	0.09±0.06	82.2%	12.0%	5.8%	17.5%	74.8%	7.6%	56.5%	37.0%	6.5%
YT	2013	0.24±0.06	0.12±0.12	0.11±0.07	76.0%	18.1%	5.9%	14.7%	78.9%	6.4%	48.2%	45.7%	6.1%
	2018	0.21±0.06	0.11±0.11	0.09±0.07	79.9%	14.7%	5.4%	14.9%	78.4%	6.7%	50.4%	43.5%	6.0%

Since the OH + NO_2 and $hetN_2O_5$ reactions are the major pathways affecting nitrate formation, we analyzed the diurnal variations in these two TNO_3 formation reactions in the NCP in detail. Figure 7 shows the average diurnal variations in the TNO_3 production rates via the different pathways in Qingdao and Beijing. We found that the OH + NO_2 reaction pathway exhibited similar diurnal characteristics in these two cities. Specifically, from nighttime to the early morning (0:00 to 8:00), the reaction rate under this pathway remained almost zero because of the lack of photochemical processes that generate OH radicals, which are limited by solar radiation (Liu et al., 2020; Sun et al., 2022; Tan et al., 2021). Observational data from the Pearl River Delta region support this result, showing that OH radicals only start to accumulate significantly after 6:00 AM (Hofzumahaus et al., 2009; Lu et al., 2012). From approximately 8:00 AM, the reaction rate rapidly increased, reaching a peak between 11:00 and 13:00 at approximately 0.4 ppb/h (approximately 2.8 μg/m^3/h), similar to findings for the NCP and Shanghai (Tan et al., 2021; Sun et al., 2022; Liu et al., 2020). The reaction rate decreased with decreasing sunlight during the afternoon and returned to low levels at night. Compared with those during the winter of 2013, the peak reaction rates of the OH pathway slightly decreased in both Qingdao and Beijing in 2018, decreasing from 0.43 to 0.42 ppb/h and 0.45 to 0.44 ppb/h in Qingdao and Beijing, respectively. The contributions of the OH + NO_2 reaction pathway to TNO_3 formation ranged from 90.2%–95.1% and 75.8%–82.2% in inland Beijing and coastal Qingdao, respectively, during the daytime, while the other cities in the NCP

https://doi.org/10.5194/egusphere-2024-3044
Preprint. Discussion started: 30 October 2024

exhibited similar diurnal variations. Therefore, the OH + NO_2 reaction pathway dominated during the daytime in both the inland and coastal cities.

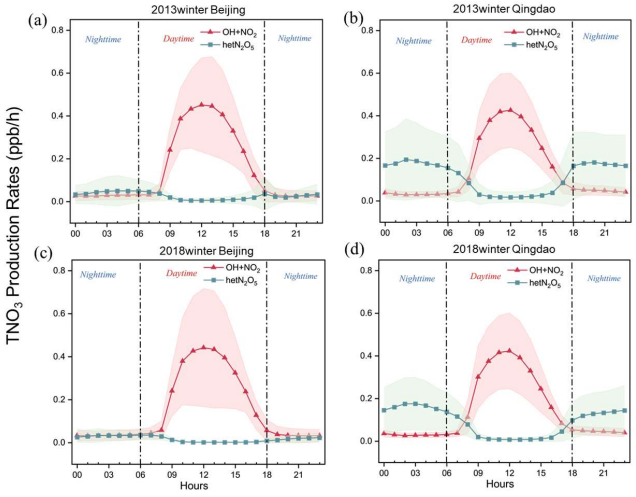

Figure 7 Average diurnal variation in the TNO_3 production rate under the different pathways (daytime: 06:00–18:00 BJT; nighttime: 18:00–06:00 BJT): (a) Beijing, 2013; (b) Qingdao, 2013; (c) Beijing, 2018; (d) Qingdao, 2018

At night, the hetN_2O_5 reaction pathway notably affected TNO_3 formation. The rate of the hetN_2O_5 reaction pathway also showed similar bimodal diurnal variations in Qingdao and Beijing. However, the peak values occurred at 2:00 and 20:00 in Qingdao, with much higher peak values than those in Beijing, where the peak values occurred from 4:00–5:00 and at 18:00. The hetN_2O_5 reaction rate was relatively high at night but decreased rapidly by early morning, reaching its lowest point during the daytime (9:00 to 16:00). This occurred because the N_2O_5 hydrolysis reaction depends heavily on NO_3 radicals and N_2O_5, which are stable only in weak-sunlight environments (Tie et al., 2003b; Tie et al., 2003a; Atkinson et al., 2004).

High concentrations of NO_2 and O_3, which are precursors for N_2O_5, are key in this process (Dentener and Crutzen, 1993):

$$NO_2 + O_3 \rightarrow NO_3 + O_2 \quad \text{(R8)}$$

$$NO_3 + NO_2 \leftrightharpoons N_2O_5 \quad \text{(R9)}$$

https://doi.org/10.5194/egusphere-2024-3044
Preprint. Discussion started: 30 October 2024

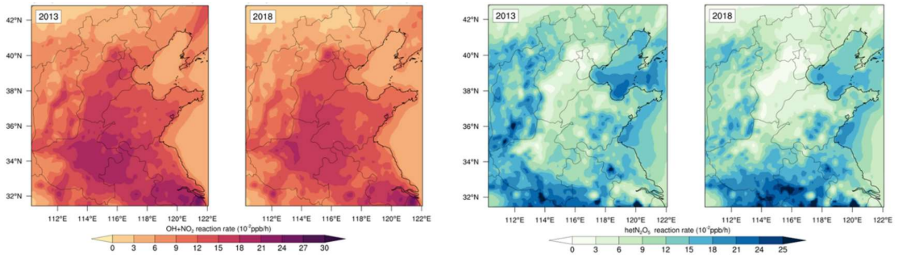

Figure 8 Spatial distributions of the mean reaction rates for the nitrate formation pathways (OH + NO_2 and hetN_2O_5) in the NCP during the winters of 2013 and 2018.

However, owing to high photolysis during the day, NO_3 radicals and N_2O_5 can accumulate only at night (Zhao et al., 2023; Atkinson et al., 2004). In Beijing, the hetN_2O_5 reaction rate was relatively low, with a peak value of only 0.03 ppb/h and a nighttime contribution rate of 46.9%. However, it could contribute up to 56–97% to nitrate formation in Beijing on polluted days with high NH_3 concentrations (He et al., 2018). In contrast, Qingdao exhibited a peak hetN_2O_5 reaction rate of 0.2 ppb/h (approximately 1.4 μg/m^3/h) at night, with an average contribution of 75.2%. This was primarily due to the higher N_2O_5 concentrations and RH levels in Qingdao than in Beijing, as detailed in section 3.5.3. The other inland cities exhibited diurnal variations similar to those in Beijing, whereas the coastal cities showed trends similar to those in Qingdao. Compared with those during the winter of 2013, the reaction rates of the hetN_2O_5 pathway in both cities during the winter of 2018 decreased, from 0.19 to 0.18 ppb/h in Qingdao and from 0.07 to 0.03 ppb/h in Beijing. Through comparative analysis, we found significant variations in the nitrate formation pathways between the coastal and inland areas, particularly in the hetN_2O_5 reaction rate, as shown in Figure 8. Further exploration of these variations is needed to better understand the marine–land differences in atmospheric nitrogen transformation.

3.4 Assessment of the simulated nitrate formation reactions via the isotopic method

https://doi.org/10.5194/egusphere-2024-3044
Preprint. Discussion started: 30 October 2024

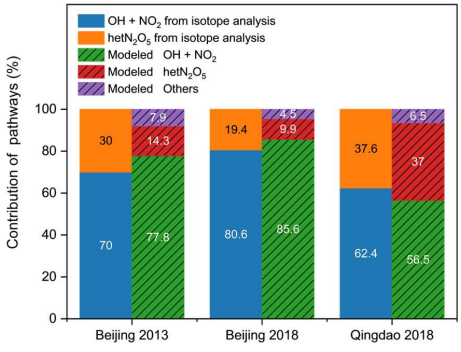

Figure 9 Comparison of the contributions of the atmospheric NO_3^- formation pathways based on the dual-isotope results and model simulations for Beijing in 2013 and 2018 and for Qingdao in 2018.

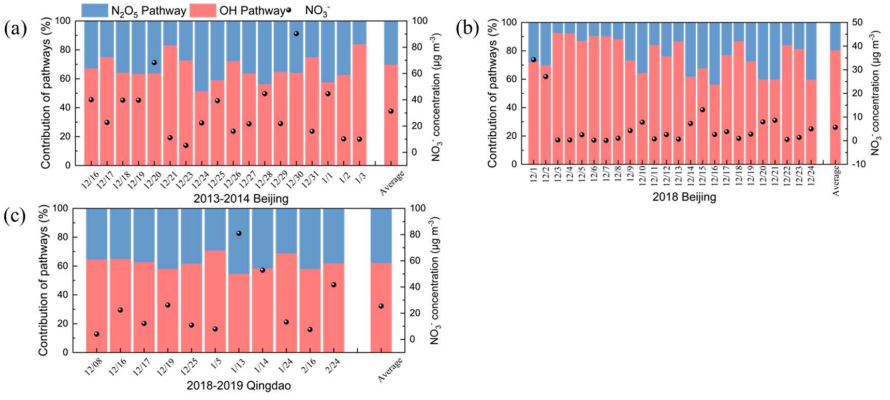

Figure 10 Time series of the contributions of the atmospheric NO_3^- formation pathways based on the dual-isotope results for Beijing in 2013 (a), 2018 (b), and Qingdao in 2018 (c)

To verify the accuracy of the simulated nitrate formation reactions, we conducted an isotopic analysis for the cities of Qingdao and Beijing. By comparing the isotopic data and model simulation results for 2013 and 2018 (Figure 9), we found high consistency in the contributions of the OH + NO_2 and hetN_2O_5 pathways to nitrate formation between these two methods, with differences ranging from 0.6% to 15.7%. The results validated the reliability of the simulated reaction pathways. The isotopic analysis also revealed that the contribution of the OH + NO_2 reaction pathway was significantly greater in Beijing than in Qingdao (Figure 10). The data for 2018 revealed that the contribution rate of the OH + NO_2 pathway in Beijing was 80.6%, which was significantly higher than that of 62.4% reported for Qingdao. Moreover, the contribution of the hetN_2O_5 pathway in Qingdao (37.0%) was greater than that in Beijing (19.4%), verifying the regional difference in nitrate formation pathways between inland and coastal cities. Additionally, the isotopic analysis indicated that the contribution of the OH + NO_2 reaction pathway

https://doi.org/10.5194/egusphere-2024-3044
Preprint. Discussion started: 30 October 2024

increased in Beijing, from 70.0% in 2013 to 80.6% in 2018, which is consistent with the model simulation results. In summary, both the model simulations and isotopic analysis results revealed that nitrate formation processes depend on different reaction pathways in inland and coastal areas.

3.5 Factors influencing nitrate formation pathways

Since the nitrate formation pathways exhibited coastal–inland differences, we further investigated the influence of several key factors on these pathways ($OH + NO_2$; $het N_2O_5$), including NH_3, NO_2, OH, O_3, RH, NO, and N_2O_5, and explored the reasons for the observed coastal–inland differences in nitrate formation.

3.5.1 Influence of NH_3 on nitrate formation

The reaction of NH_3 with nitric acid (HNO_3) to form ammonium nitrate (NH_4NO_3) is an important process in the formation of atmospheric aerosols. In the absence of sufficient NH_3, it first reacts with H_2SO_4 to form $(NH_4)_2SO_4$ and then with HNO_3 to form NH_4NO_3 (Zhai et al., 2021). This process highlights the importance of NH_3 in the formation of nitrates. Therefore, we examined the impact of NH_3 on the formation of nitrates. The gas ratio (GR) (Fu et al., 2020; Ansari and Pandis, 1998) was used to study whether NH_3 limits nitrate formation. The GR can be calculated as follows:

$$GR = \frac{([NH_3] + [NH_4^+]) - 2 \times [SO_4^{2-}]}{[NO_3^-] + [HNO_3]}$$

When the GR exceeds 1, the NH_3 concentration in the atmosphere is sufficient. A GR value between 0 and 1 indicates NH_3-neutral conditions, whereas a value less than 0 suggests NH_3-poor conditions, thus limiting NO_3^- formation due to insufficient NH_3. In the NCP region, the GR values were generally greater than 2 in 2013 and 2018 (Figure 11(a)), indicating that the region mainly exhibited a state of sufficient NH_3. Similar phenomena have also been observed by other researchers in the NCP region (Zhai et al., 2021; Xu et al., 2019c; Li et al., 2018). Therefore, in the NCP region, the formation of NH_4NO_3 is not limited by NH_3 in terms of supply.

https://doi.org/10.5194/egusphere-2024-3044
Preprint. Discussion started: 30 October 2024

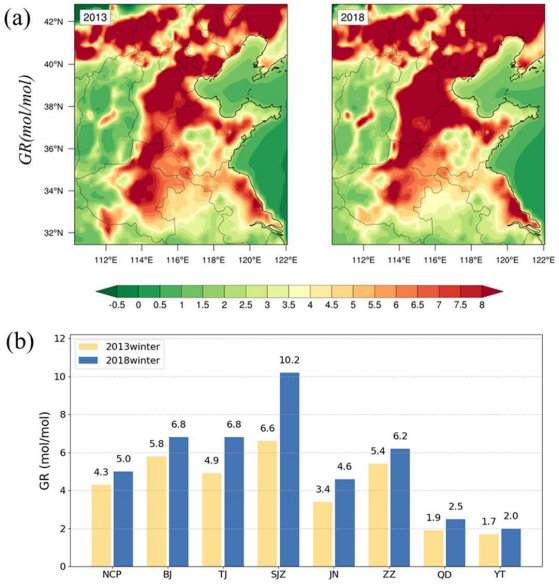

Figure 11 (a) Spatial distribution of the GR in the NCP (2013, 2018); (b) the GR in the NCP and seven major cities (2013, 2018)

The GR in 2018 was greater than that in 2013 because of the minimal changes in NH_3 emissions and the significant reduction in sulfate and slight reduction in nitrate in $PM_{2.5}$ (Figure 11(b)), indicating an increasing surplus of NH_3. This can be verified from an emission perspective, the total ammonia emissions in China increased from 9.64 to 9. 75 Tg from 2013–2015 and then gradually decreased to 9.12 Tg by 2018 (Liao et al., 2022). Additionally, there are coastal–inland differences in NH_3 surplus levels. Notably, the NH_3 surplus ratio was consistently greater than 3.4 in inland regions, while it ranged from 1.7 to 2.5 in coastal cities. This difference was primarily due to the more intensive use of fertilizers and high NH_3 emissions from livestock in inland areas.

The NH_3 supply was relatively high in the NCP region, but its impact on the increase in the nitrate proportion in $PM_{2.5}$ was not significant (Wang et al., 2023). However, Zhai et al. (2021) reported that controlling NH_3 emissions could effectively reduce the nitrate content in $PM_{2.5}$ in NH_3-rich atmospheres. Notably, when NH_3 is abundant, NO_3^- formation is constrained primarily by the conversion of HNO_3 from the gas phase to the particulate phase (Sun et al., 2022; Zhai et al., 2021). Our simulations revealed that the reduction in sulfates resulted in an excess of NH_3, which in turn promoted the partitioning of more nitrates into the particulate phase, increasing from 88.5% in 2013 to 91.7% in 2018 (Figure S2). This process not only affects the chemical composition of $PM_{2.5}$ but also significantly extends the

https://doi.org/10.5194/egusphere-2024-3044
Preprint. Discussion started: 30 October 2024

residence time of nitrates in the atmosphere because particulate nitrate exhibits a longer lifespan than that of gaseous HNO_3 (several days versus a few hours) (Liang et al., 1998; Brown et al., 2004; Millet et al., 2004), thereby increasing the risk of prolonged haze pollution.

In summary, NH_3 plays a crucial role in nitrate formation by affecting gas–to–particle conversion of HNO_3 in the NCP region, although it is sufficient. Additionally, changes in NH_3 emissions and regional land–ocean differences influence the generation and distribution of nitrates.

3.5.2 Factors influencing the OH + NO_2 reaction rate

As previously mentioned, the OH + NO_2 reaction significantly contributed to TNO_3 formation, with the OH and NO_2 concentrations serving as key factors. The NO_2 concentration in the NCP was 30.3 μg/m^3 during the winter of 2013 and decreased to 24.7 μg/m^3 during the winter of 2018, and its concentration remained several orders of magnitude greater than that of OH radicals. Figure S3 shows that the NO_2/OH molar ratio in the NCP region generally exceeded 10^8, indicating that the NO_2 concentration was still sufficient under emission reduction. Therefore, the reaction primarily depended on the OH radical concentration. Next, we examined the impact of the OH radical concentration on the reaction rate. OH radicals are produced primarily via photochemical reactions, such as the decomposition of HONO into OH and NO under sunlight (Song et al., 2023), which can account for 20% to 90% of the total primary production of OH radicals (Song et al., 2023; Xue et al., 2020; Kim et al., 2014). Additionally, OH radicals can also be produced indirectly via O_3 photolysis in the presence of water vapor (Fu et al., 2020; Kim et al., 2014).

Table 4 Observations and CMAQ model simulation results for the winter OH radical concentration

Species	Location	Obs. period	Obs. average	Sim. average	Reference
OH (10^6 cm^{-3})	Huairou_Beijing (40.41°N, 116.68°E)	Jan-Mar, 2016	Peak 2.4	Peak 0.8	Tan et al. (2018)
	Beijing PKU (40°N, 116.3°E)	Winter, 2017	Peak1.5 ~ 2.0 Daily average 0.3	Peak 0.8 Daily average 0.2	Ma et al. (2019)

We compare the simulated and observed OH radical concentrations in Table 4. The simulated daily average OH radical concentrations were relatively close to the observations. However, the peak concentrations of OH radicals were lower than those observed. Underprediction of the OH peak concentration is a common issue in current model simulations (Czader et al., 2013; Stone et al., 2012; Xue et al., 2020). Although the CMAQ model often underestimates high daytime concentrations (Czader et al., 2013), it satisfactorily captures the diurnal variation in OH radicals, likely because it

https://doi.org/10.5194/egusphere-2024-3044
Preprint. Discussion started: 30 October 2024

underestimates HONO concentrations (Zhang et al., 2023b). The data (Figure 12 a-c) revealed that the peak value of OH radicals in Beijing significantly increased by 0.98×10^6 molecules cm^{-3} in 2018 compared with that in 2013. A similar trend was observed in Qingdao, with an increase of 0.58×10^6 molecules cm^{-3}. The GEOS-Chem simulations of Zhang et al. (2023a) also indicated a stable upward trend in OH radical concentrations across the NCP from 2014 to 2017, ranging from 0.05 to 0.17×10^6 molecules cm^{-3} a^{-1}. Our study data suggested that despite China's emission reduction measures, these efforts did not effectively control OH radical concentrations. The continuous increase in OH radicals accelerated the nitrate formation rate via the OH + NO_2 pathway.

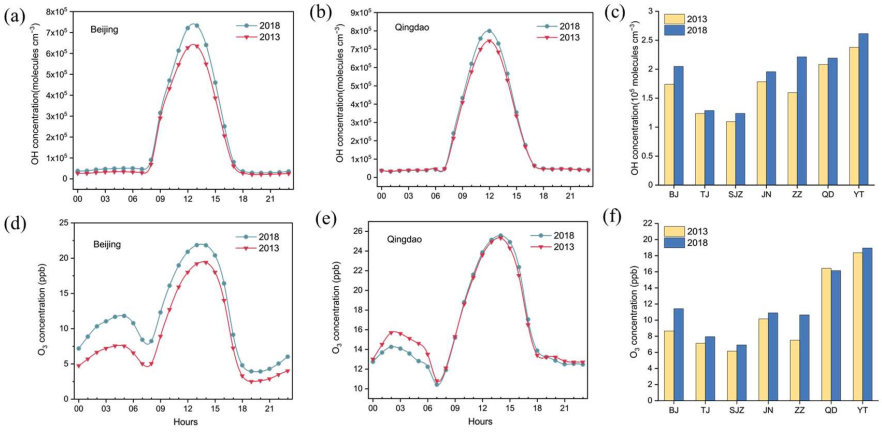

Figure 12 Diurnal variations in OH radicals and O_3 in Beijing and Qingdao and average concentrations across seven major cities in the NCP (2013, 2018): (a) Diurnal variation in OH radicals in Beijing, (b) diurnal variation in OH radicals in Qingdao, (c) average OH radical concentration in the seven cities, (d) diurnal variation in O_3 in Beijing, (e) diurnal variation in O_3 in Qingdao, and (f) average O_3 concentration in the seven cities

One of the primary pathways for the production of OH radicals is the photolysis of nitrous acid (HONO) in the tropospheric atmosphere. This photolytic reaction is can be expressed as:

$$HONO + h\nu\ (\lambda < 400nm) \rightarrow OH + NO \qquad (R10)$$

However, the data indicated that the HONO concentration decreased between 2013 and 2018 (Figure 13), suggesting that this production pathway did not significantly contribute to the increase in the OH radical concentration.

In atmospheric chemistry, another source of OH is the reaction between water vapor (H_2O) and excited oxygen atoms ($O(^1D)$). Notably, excited oxygen atoms are typically produced via O_3 photolysis (Kim et al., 2014; Tan et al., 2019).

https://doi.org/10.5194/egusphere-2024-3044
Preprint. Discussion started: 30 October 2024

$O_3 + h\nu$ ($\lambda < 340$mm) $\rightarrow O_2 + O(^1D)$ (R11)

Subsequently, the excited oxygen atoms ($O(^1D)$) react with water vapor to produce OH radicals.

$H_2O + O(^1D) \rightarrow 2OH$ (R12)

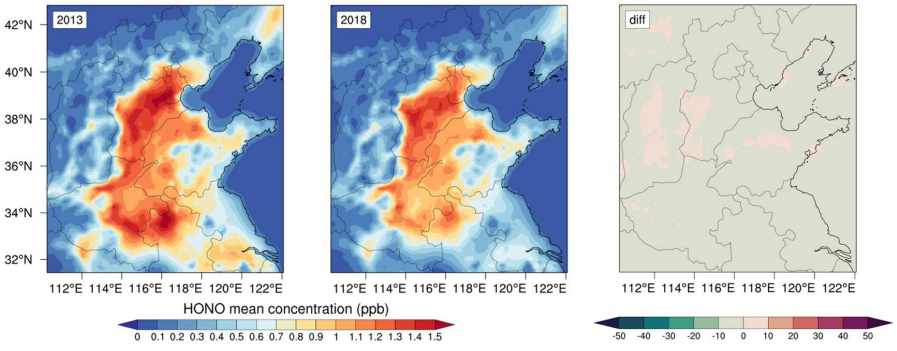

Figure 13 Changes in the HONO concentration in the NCP region during the winters of 2013 and 2018

Therefore, O_3 photolysis plays an indirect but crucial role in their formation. O_3 can oxidize NO to NO_2, which then reacts with OH radicals to form HNO_3, significantly influencing the OH + NO_2 pathway. As shown in Figure 12(d-f), the increase in the O_3 concentration indirectly increased the OH + NO_2 reaction rate for nitrate formation. This effect was greater in the inland cities, where the increase in the O_3 concentration was greater than that in the coastal cities, leading to a greater contribution of the OH + NO_2 pathway. Thus, the OH and O_3 concentrations collectively affect the formation rate, and their concentration variation affects the contribution of the OH + NO_2 pathway to nitrate formation. Although NO_2 emissions decreased, the excess NO_2 concentration indicated that the OH + NO_2 reaction rate remained relatively unchanged, which depends on OH and O_3 levels.

3.5.3 Factors influencing hetN_2O_5 reaction rates

The heterogeneous N_2O_5 reaction is also a major pathway for nitrate formation and is influenced by many factors, including the N_2O_5 concentration, aerosol surface area, and absorption coefficient of N_2O_5(γN_2O_5). The value of γN_2O_5 varies widely, ranging from an extremely low value of 10^{-4} to a relatively high value of 0.1 (Wang et al., 2023), demonstrating its high variability. Experimental results have indicated that environmental factors, such as temperature and humidity, as well as the composition of aerosols (such as NO_3^-, Cl^-, and SO_4^{2-}), the liquid water content in aerosols, the presence of organic compounds, and the mixing state of aerosols, are critical factors influencing γN_2O_5 (Folkers et al., 2003; Mitroo et al., 2019; Thornton and Abbatt, 2005; Wahner et al., 1998; Wang et al., 2020a). These factors

https://doi.org/10.5194/egusphere-2024-3044
Preprint. Discussion started: 30 October 2024

collectively influence the reaction rate and yield of heterogeneous N_2O_5 reactions.

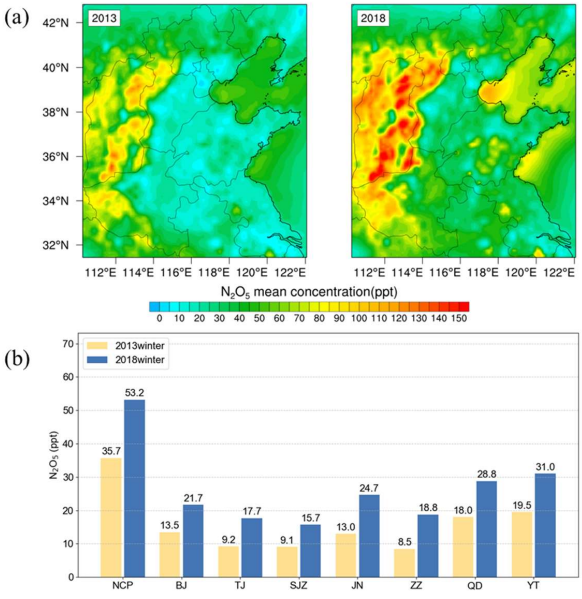

Figure 14 (a) Spatial distributions of average N_2O_5 concentrations in the NCP in 2013 and 2018; (b) average N_2O_5 concentrations in the NCP and seven major cities in 2013 and 2018

With increasing concentration of atmospheric O_3 (as shown in Figure 12(f)), the generation rate of N_2O_5 significantly increased. Consequently, the average N_2O_5 concentration in the NCP was 35.7 ppt in 2013 and increased to 53.2 ppt in 2018 (Figure 14). From a spatial distribution perspective, the N_2O_5 concentrations are generally higher in ocean areas and western mountainous regions than in central inland areas. Thus, the N_2O_5 concentrations in the coastal cities were generally higher than those in the inland cities. Therefore, we reasoned that the decreased reaction rate of heterogeneous N_2O_5 was influenced more by other factors, such as the surface area of aerosol particles and RH. The total dry surface area of particles in the CMAQ model is calculated as the sum of the modal dry surface areas (SRFATKN, SRFACC, and SRFCOR), corresponding to particles in the Aitken, accumulation, and coarse modes, respectively (Bergin et al., 2022). During the winter of 2013 in the NCP, the average SRF value was 689 $\mu m^2/cm^3$, which decreased to 425 $\mu m^2/cm^3$ during the winter of 2018, a reduction of 38.3%. This significant reduction in the aerosol surface area likely contributed to the observed decrease in the reaction rate of heterogeneous N_2O_5. Air quality monitoring data also verified that PM_{10} decreased by 20% and that $PM_{2.5}$ decreased by 28% in China from 2014 to 2018 (Fan et al., 2020a). Compared with that in 2013, the RH in the NCP decreased by 3.1% in 2018 (Figure S4). However, the sensitivity experiments revealed

https://doi.org/10.5194/egusphere-2024-3044
Preprint. Discussion started: 30 October 2024

that both the N_2O_5 reaction rate and its contribution to total nitrates remained essentially unchanged when the humidity decreased by 10%. This indicated that humidity changes were not the main factor influencing the decrease in the reaction rate of heterogeneous N_2O_5 in the NCP. Therefore, we considered that the reduction in the $PM_{2.5}$ concentration was a major factor contributing to the decrease in the hetN_2O_5 generation rate.

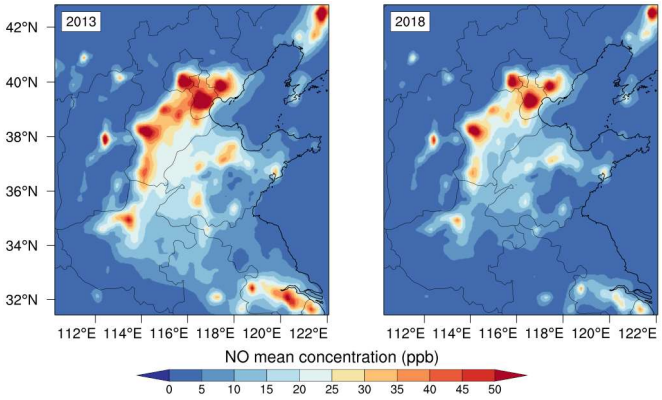

Figure 15 Spatial distribution of the average NO concentrations in the NCP (2013, 2018)

We then investigated the differences in the spatial distribution of N_2O_5 and found that NO played a significant role in the spatial distribution of N_2O_5. In urban areas, especially during severe haze nighttime periods, the rapid titration of NO with O_3 led to near-zero concentrations of surface O_3 (Zang et al., 2022), thereby inhibiting the in situ generation of NO_3 radicals and N_2O_5 (Zhao et al., 2023). Therefore, high surface NO concentrations are unfavorable for the in situ generation of NO_3 radicals and N_2O_5. As shown in Figure 15, the NO concentrations were high in central inland areas and low in coastal and western mountainous areas, which explained the low N_2O_5 concentrations in inland cities. Additionally, observations have shown that the lifetime of NO_3 radicals in marine atmospheres could reach 30 minutes, which is longer than 1 minute in inland atmospheres (Crowley et al., 2011), also contributing to high N_2O_5 concentrations in coastal cities. This difference may be due to the low NOx mixing ratio in marine air masses. Observations in Hebei Province also revealed low N_2O_5 concentrations in summer, with lifetimes ranging from 0.1 to 10 minutes (Tham et al., 2018). Therefore, the spatial differences in hetN_2O_5 reaction rates depend on NO and the lifetime of NO_3 radicals, providing insights into the complexity and regional characteristics of atmospheric chemical processes.

https://doi.org/10.5194/egusphere-2024-3044
Preprint. Discussion started: 30 October 2024

3.6 Impact of reducing NOx and VOCs emissions on the nitrate concentration

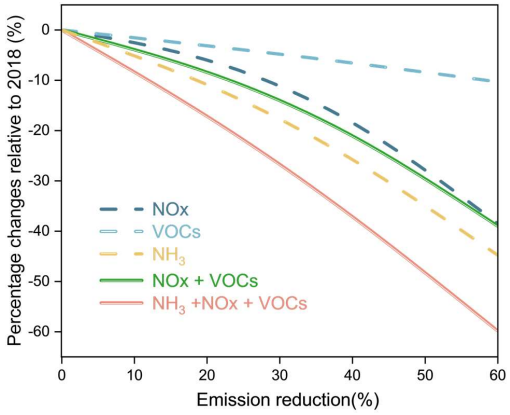

Figure 16 Variation in $PM_{2.5}$ nitrate percentages in response to emission reduction within the North China Plain relative to the winter of 2018.

Reducing the nitrate content in $PM_{2.5}$ is crucial for improving the air quality in China, especially in winter when pollution levels peak. As discussed above, O_3 and OH radicals play central roles in the OH + NO_2 pathway of nitrate formation, whereas the formation of N_2O_5 relies on the synergistic action of NO_2 and O_3. Effective control strategies must target key factors, such as OH radicals, O_3, and the photochemical reactions of NOx and VOCs. However, a previous study revealed that even with a 30% reduction in VOCs and NOx emissions, the winter nitrate concentration in $PM_{2.5}$ in the NCP decreased by only 8.6% (Fu et al., 2020). NH_3 plays a crucial role in the gas-to-particle conversion process of HNO_3 in the NCP region. Therefore, we designed single and combined pollutant reduction strategies for NH_3, NOx, and VOCs to examine the effects of the emission of these species on nitrate in $PM_{2.5}$.

The emission reduction results (Figure 16) revealed that single VOCs reduction imposed a limited effect on controlling nitrate. When emissions were reduced by 60%, nitrate decreased by only 10.3%. In contrast, NOx reduction imposed a greater effect on controlling nitrate. When NOx emissions were reduced by 60%, nitrate decreased by approximately 38.4%. However, this simulated reduction level was significantly greater than the current NOx reduction outcomes in China. When both NOx and VOCs were reduced, the effect slightly increased to 39.0%. When NH_3 emissions were reduced by 60%, nitrate decreased by 44.8%. The best results were achieved when NH_3, VOCs, and NOx were jointly reduced by 60%, and nitrate decreased by 59.8%. These findings suggest that for effective control of nitrate concentrations, combined reduction in NOx, VOCs, and NH_3 emissions is necessary. To reduce the nitrate

https://doi.org/10.5194/egusphere-2024-3044
Preprint. Discussion started: 30 October 2024

concentration via a single emission source, the most effective measure would be to decrease NH_3 emissions.

4 Conclusion

In this study, nitrate formation mechanisms and influencing factors in seven cities across the NCP during the winters of 2013 and 2018 were investigated. Our findings revealed that nitrate formation was significantly influenced by NH_3, NO_2, OH radicals, O_3, NO, and N_2O_5, with distinct differences between regions. In inland cities, the OH + NO_2 reaction pathway dominated, contributing 63.7%–85.6% to nitrate formation. This was largely driven by the increased concentrations of OH radicals and O_3, resulting in a 7.6% greater contribution of this pathway in inland cities in 2018 than in 2013. In contrast, coastal cities exhibited a greater contribution of the hetN_2O_5 pathway (37.0% to 45.7%) because of the higher N_2O_5 concentrations and longer NO_3 radical lifetimes. High NO concentrations in inland areas facilitate O_3 titration, inhibiting N_2O_5 formation and further differentiating the nitrate formation processes between the two regions.

Our emission reduction experiments demonstrated the critical need for a comprehensive and coordinated approach to effectively mitigate nitrate pollution in the NCP. A 60% reduction in NO_x emissions alone led to a 38.4% decrease in nitrate concentrations. However, combined reduction in NO_x, VOCs, and NH_3 yielded a greater decrease of 59.8%. These results highlight the necessity of region-specific, multipollutant control strategies to achieve significant reductions in $PM_{2.5}$ nitrate levels and alleviate associated health risks. Furthermore, our study increases the understanding of atmospheric nitrogen chemistry, providing critical insights for developing more targeted and effective measures to mitigate nitrate pollution and improve the air quality.

https://doi.org/10.5194/egusphere-2024-3044
Preprint. Discussion started: 30 October 2024

Declaration of Competing Interest

The authors declare that they have no known competing financial interests or personal relationships that could have appeared to influence the work reported in this paper.

CRediT authorship contribution statement

Zhenze Liu: Visualization, Formal analysis, Writing – original draft. **Xiaohuan Liu**: Project administration, Writing – review & editing. **Yuanze Ni**: Validation.. **Likun Xue**: Resources. **Jianhua Qi**: Conceptualization, Methodology, Writing - review & editing

Data availability

The data will be made available upon request.

Acknowledgments

This work was financially supported by the Key Program of the National Natural Science Foundation of China (42430606). The authors are extremely grateful to Prof. Xiaodong Li for his help with the nitrate data.

https://doi.org/10.5194/egusphere-2024-3044
Preprint. Discussion started: 30 October 2024

References

Ansari, A. S. and Pandis, S. N.: Response of Inorganic PM to Precursor Concentrations, Environmental Science & Technology, 32, 2706-2714, doi:10.1021/es971130j, 1998.

Appel, K. W., Bash, J. O., Fahey, K. M., Foley, K. M., and Wong, D. C.: The Community Multiscale Air Quality (CMAQ) Model Versions 5.3 and 5.3.1: System Updates and Evaluation, 2020.

Athanasopoulou, E., Tombrou, M., Pandis, S. N., and Russell, A. G.: The role of sea-salt emissions and heterogeneous chemistry in the air quality of polluted coastal areas, Atmos. Chem. Phys., 8, 5755-5769, doi:10.5194/acp-8-5755-2008, 2008.

Atkinson, R.: Atmospheric chemistry of VOCs and NOx, Atmospheric Environment, 34, 2063-2101, doi:10.1016/S1352-2310(99)00460-4, 2000.

Atkinson, R., Baulch, D. L., Cox, R. A., Crowley, J. N., Hampson, R. F., Hynes, R. G., Jenkin, M. E., Rossi, M. J., and Troe, J.: Evaluated kinetic and photochemical data for atmospheric chemistry: Volume I - gas phase reactions of Ox, HOx, NOx and SOx species, Atmos. Chem. Phys., 4, 1461-1738,doi:10.5194/acp-4-1461-2004, 2004.

Bergin, R. A., Harkey, M., Hoffman, A., Moore, R. H., Anderson, B., Beyersdorf, A., Ziemba, L., Thornhill, L., Winstead, E., Holloway, T., and Bertram, T. H.: Observation-based constraints on modeled aerosol surface area: implications for heterogeneous chemistry, Atmos. Chem. Phys., 22, 15449-15468, doi:10.5194/acp-22-15449-2022, 2022.

Brown, S. S., Dibb, J. E., Stark, H., Aldener, M., Vozella, M., Whitlow, S., Williams, E. J., Lerner, B. M., Jakoubek, R., Middlebrook, A. M., DeGouw, J. A., Warneke, C., Goldan, P. D., Kuster, W. C., Angevine, W. M., Sueper, D. T., Quinn, P. K., Bates, T. S., Meagher, J. F., Fehsenfeld, F. C., and Ravishankara, A. R.: Nighttime removal of NOx in the summer marine boundary layer, Geophysical Research Letters, 31, doi:10.1029/2004GL019412, 2004.

Cao, J., Tie, X., Dabberdt, W. F., Jie, T., Zhao, Z., An, Z., Shen, Z., and Feng, Y.: On the potential high acid deposition in northeastern China, Journal of Geophysical Research: Atmospheres, 118, 4834-4846, doi:10.1002/jgrd.50381, 2013.

Casciotti, K. L., Sigman, D. M., Hastings, M. G., Böhlke, J. K., and Hilkert, A.: Measurement of the Oxygen Isotopic Composition of Nitrate in Seawater and Freshwater Using the Denitrifier Method, Analytical Chemistry, 74, 4905-4912, doi:10.1021/ac020113w, 2002.

Chen, C., Huang, L., Shi, J., Zhou, Y., Wang, J., Yao, X., Gao, H., Liu, Y., Xing, J., and Liu, X.:

https://doi.org/10.5194/egusphere-2024-3044
Preprint. Discussion started: 30 October 2024

Atmospheric outflow of anthropogenic iron and its deposition to China adjacent seas, Science of The Total Environment, 750, 141302, doi:10.1016/j.scitotenv.2020.141302, 2021.

Chen, D., Liu, Z., Fast, J., and Ban, J.: Simulations of sulfate-nitrate-ammonium (SNA) aerosols during the extreme haze events over northern China in October 2014, Atmos. Chem. Phys., 16, 10707-10724, doi:10.5194/acp-16-10707-2016, 2016.

Chen, X., Wang, H., Lu, K., Li, C., Zhai, T., Tan, Z., Ma, X., Yang, X., Liu, Y., Chen, S., Dong, H., Li, X., Wu, Z., Hu, M., Zeng, L., and Zhang, Y.: Field Determination of Nitrate Formation Pathway in Winter Beijing, Environmental Science & Technology, 54, 9243-9253, doi:10.1021/acs.est.0c00972, 2020.

Crowley, J. N., Thieser, J., Tang, M. J., Schuster, G., Bozem, H., Beygi, Z. H., Fischer, H., Diesch, J. M., Drewnick, F., Borrmann, S., Song, W., Yassaa, N., Williams, J., Pöhler, D., Platt, U., and Lelieveld, J.: Variable lifetimes and loss mechanisms for NO_3 and N_2O_5 during the DOMINO campaign: contrasts between marine, urban and continental air, Atmos. Chem. Phys., 11, 10853-10870, doi:10.5194/acp-11-10853-2011, 2011.

Czader, B. H., Li, X., and Rappenglueck, B.: CMAQ modeling and analysis of radicals, radical precursors, and chemical transformations, Journal of Geophysical Research: Atmospheres, 118, 11,376-311,387, doi:10.1002/jgrd.50807, 2013.

Dentener, F. J. and Crutzen, P. J.: Reaction of N_2O_5 on tropospheric aerosols: Impact on the global distributions of NO x , O3, and OH, Journal of Geophysical Research: Atmospheres, 98, 7149-7163, doi:10.1029/92JD02979, 1993.

Ding, X., Qi, J., and Meng, X.: Characteristics and sources of organic carbon in coastal and marine atmospheric particulates over East China, Atmospheric Research, 228, 281-291, doi:10.1016/j.atmosres.2019.06.015, 2019.

Emery, C., Tai, E., and Yarwood, G.: Enhanced meteorological modeling and performance evaluation for two Texas ozone episodes, Prepared for the Texas natural resource conservation commission, by ENVIRON International Corporation, 2001.

Emery, C., Liu, Z., Russell, A. G., Odman, M. T., Yarwood, G., and Kumar, N.: Recommendations on statistics and benchmarks to assess photochemical model performance, Journal of the Air & Waste Management Association, 67, 582-598, doi:10.1080/10962247.2016.1265027, 2017.

Fan, H., Zhao, C., and Yang, Y.: A comprehensive analysis of the spatio-temporal variation of urban air

https://doi.org/10.5194/egusphere-2024-3044
Preprint. Discussion started: 30 October 2024

pollution in China during 2014-2018, Atmospheric Environment, 220, 117066, doi:10.1016/j.atmosenv.2019.117066, 2020a.

Fan, M.-Y., Zhang, Y.-L., Lin, Y.-C., Cao, F., Zhao, Z.-Y., Sun, Y., Qiu, Y., Fu, P., and Wang, Y.: Changes of Emission Sources to Nitrate Aerosols in Beijing After the Clean Air Actions: Evidence From Dual Isotope Compositions, Journal of Geophysical Research: Atmospheres, 125, e2019JD031998, doi:10.1029/2019JD031998, 2020b.

Folkers, M., Mentel, T. F., and Wahner, A.: Influence of an organic coating on the reactivity of aqueous aerosols probed by the heterogeneous hydrolysis of N_2O_5, Geophysical Research Letters, 30, doi:10.1029/2003GL017168, 2003.

Fu, X., Wang, T., Gao, J., Wang, P., Liu, Y., Wang, S., Zhao, B., and Xue, L.: Persistent Heavy Winter Nitrate Pollution Driven by Increased Photochemical Oxidants in Northern China, Environmental Science & Technology, 54, 3881-3889, dx.doi:10.1021/acs.est.9b07248, 2020.

He, P., Xie, Z., Yu, X., Wang, L., Kang, H., and Yue, F.: The observation of isotopic compositions of atmospheric nitrate in Shanghai China and its implication for reactive nitrogen chemistry, Science of The Total Environment, 714, 136727, doi:10.1016/j.scitotenv.2020.136727, 2020.

He, P., Xie, Z., Chi, X., Yu, X., Fan, S., Kang, H., Liu, C., and Zhan, H.: Atmospheric $\Delta^{17}O(NO_3^-)$ reveals nocturnal chemistry dominates nitrate production in Beijing haze, Atmos. Chem. Phys., 18, 14465-14476, doi:10.5194/acp-18-14465-2018, 2018.

Hofzumahaus, A., Rohrer, F., Lu, K., Bohn, B., Brauers, T., Chang, C.-C., Fuchs, H., Holland, F., Kita, K., Kondo, Y., Li, X., Lou, S., Shao, M., Zeng, L., Wahner, A., and Zhang, Y.: Amplified Trace Gas Removal in the Troposphere, Science, 324, 1702-1704,doi:10.1126/science.1164566, 2009.

Huang, L., Zhu, Y., Zhai, H., Xue, S., Zhu, T., Shao, Y., Liu, Z., Emery, C., Yarwood, G., Wang, Y., Fu, J., Zhang, K., and Li, L.: Recommendations on benchmarks for numerical air quality model applications in China-Part 1: PM2.5 and chemical species, Atmos. Chem. Phys., 21, 2725-2743, doi:10.5194/acp-21-2725-2021, 2021.

Jacobson, M. Z. and Kaufman, Y. J.: Wind reduction by aerosol particles, Geophysical Research Letters, 33, doi:10.1029/2006GL027838, 2006.

Kalkavouras, P., Bougiatioti, A., Kalivitis, N., Stavroulas, I., Tombrou, M., Nenes, A., and Mihalopoulos, N.: Regional new particle formation as modulators of cloud condensation nuclei and cloud droplet

https://doi.org/10.5194/egusphere-2024-3044
Preprint. Discussion started: 30 October 2024

number in the eastern Mediterranean, Atmos. Chem. Phys., 19, 6185-6203, doi:10.5194/acp-19-6185-2019, 2019.

Kim, S., VandenBoer, T. C., Young, C. J., Riedel, T. P., Thornton, J. A., Swarthout, B., Sive, B., Lerner, B., Gilman, J. B., Warneke, C., Roberts, J. M., Guenther, A., Wagner, N. L., Dubé, W. P., Williams, E., and Brown, S. S.: The primary and recycling sources of OH during the NACHTT-2011 campaign: HONO as an important OH primary source in the wintertime, Journal of Geophysical Research: Atmospheres, 119, 6886-6896, doi:10.1002/2013JD019784, 2014.

Kunasek, S. A., Alexander, B., Steig, E. J., Hastings, M. G., Gleason, D. J., and Jarvis, J. C.: Measurements and modeling of $\Delta^{17}O$ of nitrate in snowpits from Summit, Greenland, Journal of Geophysical Research: Atmospheres, 113, doi:10.1029/2008JD010103, 2008.

Li, H., Cheng, J., Zhang, Q., Zheng, B., Zhang, Y., Zheng, G., and He, K.: Rapid transition in winter aerosol composition in Beijing from 2014 to 2017: response to clean air actions, Atmos. Chem. Phys., 19, 11485-11499, doi:10.5194/acp-19-11485-2019, 2019.

Li, H., Zhang, Q., Zheng, B., Chen, C., Wu, N., Guo, H., Zhang, Y., Zheng, Y., Li, X., and He, K.: Nitrate-driven urban haze pollution during summertime over the North China Plain, Atmos. Chem. Phys., 18, 5293-5306, doi:10.5194/acp-18-5293-2018, 2018.

Li, R., Gao, Y., Xu, J., Cui, L., and Wang, G.: Impact of Clean Air Policy on Criteria Air Pollutants and Health Risks Across China During 2013–2021, Journal of Geophysical Research: Atmospheres, 128, e2023JD038939, doi:10.1029/2023JD038939, 2023.

Li, X., Wu, S.-P., Zhang, J., and Schwab, J. J.: Insights into factors affecting size-segregated nitrate formation in a coastal city through measurements of dual isotopes, Atmospheric Environment, 290, 119385, doi:10.1016/j.atmosenv.2022.119385, 2022.

Liang, J., Horowitz, L. W., Jacob, D. J., Wang, Y., Fiore, A. M., Logan, J. A., Gardner, G. M., and Munger, J. W.: Seasonal budgets of reactive nitrogen species and ozone over the United States, and export fluxes to the global atmosphere, Journal of Geophysical Research: Atmospheres, 103, 13435-13450, doi:10.1029/97JD03126, 1998.

Liao, W., LIU, M., HUANG, X., WANG, T., XU, Z., SHANG, F., SONG, Y., CAI, X., ZHANG, H., KANG, L., and ZHU, T.: Estimation for ammonia emissions at county level in China from 2013 to 2018, 65, 1116-1127, doi:10.1007/s11430-021-9897-3, 2022.

https://doi.org/10.5194/egusphere-2024-3044
Preprint. Discussion started: 30 October 2024

Liu, L., Bei, N., Hu, B., Wu, J., Liu, S., Li, X., Wang, R., Liu, Z., Shen, Z., and Li, G.: Wintertime nitrate formation pathways in the north China plain: Importance of N2O5 heterogeneous hydrolysis, Environmental Pollution, 266, 115287, doi:10.1016/j.envpol.2020.115287, 2020.

Liu, X., Chang, M., Zhang, J., Wang, J., Gao, H., Gao, Y., and Yao, X.: Rethinking the causes of extreme heavy winter $PM_{2.5}$ pollution events in northern China, Science of The Total Environment, 794, 148637, doi:10.1016/j.scitotenv.2021.148637, 2021.

Lu, K. D., Rohrer, F., Holland, F., Fuchs, H., Bohn, B., Brauers, T., Chang, C. C., Häseler, R., Hu, M., Kita, K., Kondo, Y., Li, X., Lou, S. R., Nehr, S., Shao, M., Zeng, L. M., Wahner, A., Zhang, Y. H., and Hofzumahaus, A.: Observation and modelling of OH and HO_2 concentrations in the Pearl River Delta 2006: a missing OH source in a VOC rich atmosphere, Atmos. Chem. Phys., 12, 1541-1569, doi:10.5194/acp-12-1541-2012, 2012.

Luecken, D. J., Yarwood, G., and Hutzell, W. T.: Multipollutant modeling of ozone, reactive nitrogen and HAPs across the continental US with CMAQ-CB6, Atmospheric Environment, 201, 62-72, doi:10.1016/j.atmosenv.2018.11.060, 2019.

Luo, L., Zhu, R.-g., Song, C.-B., Peng, J.-F., Guo, W., Liu, Y., Zheng, N., Xiao, H., and Xiao, H.-Y.: Changes in nitrate accumulation mechanisms as $PM_{2.5}$ levels increase on the North China Plain: A perspective from the dual isotopic compositions of nitrate, Chemosphere, 263, 127915, doi:10.1016/j.chemosphere.2020.127915, 2021.

Ma, X., Tan, Z., Lu, K., Yang, X., Liu, Y., Li, S., Li, X., Chen, S., Novelli, A., Cho, C., Zeng, L., Wahner, A., and Zhang, Y.: Winter photochemistry in Beijing: Observation and model simulation of OH and HO2 radicals at an urban site, Science of The Total Environment, 685, 85-95, doi:10.1016/j.scitotenv.2019.05.329, 2019.

Michalski, G., Scott, Z., Kabiling, M., and Thiemens, M. H.: First measurements and modeling of $\Delta^{17}O$ in atmospheric nitrate, Geophysical Research Letters, 30, doi:10.1029/2003GL017015, 2003.

Millet, D. B., Goldstein, A. H., Allan, J. D., Bates, T. S., Boudries, H., Bower, K. N., Coe, H., Ma, Y., McKay, M., Quinn, P. K., Sullivan, A., Weber, R. J., and Worsnop, D. R.: Volatile organic compound measurements at Trinidad Head, California, during ITCT 2K2: Analysis of sources, atmospheric composition, and aerosol residence times, Journal of Geophysical Research: Atmospheres, 109, doi:10.1029/2003JD004026, 2004.

https://doi.org/10.5194/egusphere-2024-3044
Preprint. Discussion started: 30 October 2024

Mitroo, D., Gill, T. E., Haas, S., Pratt, K. A., and Gaston, C. J.: $ClNO_2$ Production from N_2O_5 Uptake on Saline Playa Dusts: New Insights into Potential Inland Sources of $ClNO_2$, Environmental Science & Technology, 53, 7442-7452, doi:10.1021/acs.est.9b01112, 2019.

Peng, W., Zhu, B., Kang, H., Chen, K., Lu, W., Lu, C., Kang, N., Hu, J., Chen, H., and Liao, H.: Inconsistent 3-D Structures and Sources of Sulfate Ammonium and Nitrate Ammonium Aerosols During Cold Front Episodes, Journal of Geophysical Research: Atmospheres, 129, e2023JD039958, doi:10.1029/2023JD039958, 2024.

Qi, J., Yu, Y., Yao, X., Gang, Y., and Gao, H.: Dry deposition fluxes of inorganic nitrogen and phosphorus in atmospheric aerosols over the Marginal Seas and Northwest Pacific, Atmospheric Research, 245, doi:10.1016/j.atmosres.2020.105076, 2020.

Ramanathan, V. and Feng, Y.: Air pollution, greenhouse gases and climate change: Global and regional perspectives, Atmospheric Environment, 43, 37-50, doi:10.1016/j.atmosenv.2008.09.063, 2009.

Shao, P., Tian, H., Sun, Y., Liu, H., Wu, B., Liu, S., Liu, X., Wu, Y., Liang, W., Wang, Y., Gao, J., Xue, Y., Bai, X., Liu, W., Lin, S., and Hu, G.: Characterizing remarkable changes of severe haze events and chemical compositions in multi-size airborne particles (PM_1, $PM_{2.5}$ and PM_{10}) from January 2013 to 2016–2017 winter in Beijing, China, Atmospheric Environment, 189, 133-144, doi:10.1016/j.atmosenv.2018.06.038, 2018.

Sigman, D. M., Casciotti, K. L., Andreani, M., Barford, C., Galanter, M., and Böhlke, J. K.: A Bacterial Method for the Nitrogen Isotopic Analysis of Nitrate in Seawater and Freshwater, Analytical Chemistry, 73, 4145-4153, doi:10.1021/ac010088e, 2001.

Song, M., Zhao, X., Liu, P., Mu, J., He, G., Zhang, C., Tong, S., Xue, C., Zhao, X., Ge, M., and Mu, Y.: Atmospheric NOx oxidation as major sources for nitrous acid (HONO), npj Climate and Atmospheric Science, 6, 30, doi:10.1038/s41612-023-00357-8, 2023.

Stone, D., Whalley, L. K., and Heard, D. E.: Tropospheric OH and HO_2 radicals: field measurements and model comparisons, Chemical Society Reviews, 41, 6348-6404, doi:10.1039/C2CS35140D, 2012.

Sun, J., Qin, M., Xie, X., Fu, W., Qin, Y., Sheng, L., Li, L., Li, J., Sulaymon, I. D., Jiang, L., Huang, L., Yu, X., and Hu, J.: Seasonal modeling analysis of nitrate formation pathways in Yangtze River Delta region, China, Atmospheric Chemistry and Physics, 22, 12629-12646, doi:10.5194/acp-22-12629-2022, 2022.

https://doi.org/10.5194/egusphere-2024-3044
Preprint. Discussion started: 30 October 2024

Sun, Y., Jiang, Q., Wang, Z., Fu, P., Li, J., Yang, T., and Yin, Y.: Investigation of the sources and evolution processes of severe haze pollution in Beijing in January 2013, Journal of Geophysical Research: Atmospheres, 119, 4380-4398, doi:10.1002/2014JD021641, 2014.

Tan, J., Zhang, Y., Ma, W., Yu, Q., Wang, Q., Fu, Q., Zhou, B., Chen, J., and Chen, L.: Evaluation and potential improvements of WRF/CMAQ in simulating multi-levels air pollution in megacity Shanghai, China, Stochastic Environmental Research and Risk Assessment, 31, 2513-2526, doi:10.1007/s00477-016-1342-3, 2017.

Tan, Z., Wang, H., Lu, K., Dong, H., Liu, Y., Zeng, L., Hu, M., and Zhang, Y.: An Observational Based Modeling of the Surface Layer Particulate Nitrate in the North China Plain During Summertime, Journal of Geophysical Research: Atmospheres, 126, e2021JD035623, doi:10.1029/2021JD035623, 2021.

Tan, Z., Lu, K., Hofzumahaus, A., Fuchs, H., Bohn, B., Holland, F., Liu, Y., Rohrer, F., Shao, M., Sun, K., Wu, Y., Zeng, L., Zhang, Y., Zou, Q., Kiendler-Scharr, A., Wahner, A., and Zhang, Y.: Experimental budgets of OH, HO_2, and RO_2 radicals and implications for ozone formation in the Pearl River Delta in China 2014, Atmos. Chem. Phys., 19, 7129-7150, doi:10.5194/acp-19-7129-2019, 2019.

Tan, Z., Rohrer, F., Lu, K., Ma, X., Bohn, B., Broch, S., Dong, H., Fuchs, H., Gkatzelis, G. I., Hofzumahaus, A., Holland, F., Li, X., Liu, Y., Liu, Y., Novelli, A., Shao, M., Wang, H., Wu, Y., Zeng, L., Hu, M., Kiendler-Scharr, A., Wahner, A., and Zhang, Y.: Wintertime photochemistry in Beijing: observations of ROx radical concentrations in the North China Plain during the BEST-ONE campaign, Atmos. Chem. Phys., 18, 12391-12411, doi:10.5194/acp-18-12391-2018, 2018.

Tegen, I., Koch, D., Lacis, A. A., and Sato, M.: Trends in tropospheric aerosol loads and corresponding impact on direct radiative forcing between 1950 and 1990: A model study, Journal of Geophysical Research: Atmospheres, 105, 26971-26989, doi:10.1029/2000JD900280, 2000.

Tham, Y. J., Wang, Z., Li, Q., Wang, W., Wang, X., Lu, K., Ma, N., Yan, C., Kecorius, S., Wiedensohler, A., Zhang, Y., and Wang, T.: Heterogeneous N2O5 uptake coefficient and production yield of ClNO2 in polluted northern China: roles of aerosol water content and chemical composition, Atmos. Chem. Phys., 18, 13155-13171, doi:10.5194/acp-18-13155-2018, 2018.

Thornton, J. A. and Abbatt, J. P. D.: N2O5 Reaction on Submicron Sea Salt Aerosol: Kinetics, Products, and the Effect of Surface Active Organics, The Journal of Physical Chemistry A, 109, doi:10004-10012, 10.1021/jp054183t, 2005.

https://doi.org/10.5194/egusphere-2024-3044
Preprint. Discussion started: 30 October 2024

Tie, X., Wu, D., and Brasseur, G.: Lung cancer mortality and exposure to atmospheric aerosol particles in Guangzhou, China, Atmospheric Environment, 43, 2375-2377, doi:10.1016/j.atmosenv.2009.01.036, 2009.

Tie, X., Madronich, S., Walters, S., Zhang, R., Rasch, P., and Collins, W.: Effect of clouds on photolysis and oxidants in the troposphere, Journal of Geophysical Research: Atmospheres, 108, doi:10.1029/2003JD003659, 2003a.

Tie, X., Emmons, L., Horowitz, L., Brasseur, G., Ridley, B., Atlas, E., Stround, C., Hess, P., Klonecki, A., Madronich, S., Talbot, R., and Dibb, J.: Effect of sulfate aerosol on tropospheric NOx and ozone budgets: Model simulations and TOPSE evidence, Journal of Geophysical Research: Atmospheres, 108, doi:10.1029/2001JD001508, 2003b.

US-EPA: Guidance on the use of models and other analyses for demonstrating attainment of air quality goals for ozone, $PM_{2.5}$, and regional haze, US Environmental Protection Agency, Office of Air Quality Planning and Standards, 2007.

Wahner, A., Mentel, T. F., Sohn, M., and Stier, J.: Heterogeneous reaction of N_2O_5 on sodium nitrate aerosol, Journal of Geophysical Research: Atmospheres, 103, 31103-31112, doi:10.1029/1998JD100022, 1998.

Walters, W. W. and Michalski, G.: Theoretical calculation of oxygen equilibrium isotope fractionation factors involving various NOy molecules, OH, and H_2O and its implications for isotope variations in atmospheric nitrate, Geochimica et Cosmochimica Acta, 191, 89-101, doi:10.1016/j.gca.2016.06.039, 2016.

Wang, F., An, J., Li, Y., Tang, Y., Lin, J., Qu, Y., Chen, Y., Zhang, B., and Zhai, J.: Impacts of uncertainty in AVOC emissions on the summer ROx budget and ozone production rate in the three most rapidly-developing economic growth regions of China, Advances in Atmospheric Sciences, 31, 1331-1342, doi:10.1007/s00376-014-3251-z, 2014.

Wang, H., Lu, K., Tan, Z., Chen, X., Liu, Y., and Zhang, Y.: Formation mechanism and control strategy for particulate nitrate in China, Journal of Environmental Sciences, 123, 476-486, doi:10.1016/j.jes.2022.09.019, 2023.

Wang, H., Chen, X., Lu, K., Tan, Z., Ma, X., Wu, Z., Li, X., Liu, Y., Shang, D., Wu, Y., Zeng, L., Hu, M., Schmitt, S., Kiendler-Scharr, A., Wahner, A., and Zhang, Y.: Wintertime N_2O_5 uptake coefficients over

https://doi.org/10.5194/egusphere-2024-3044
Preprint. Discussion started: 30 October 2024

the North China Plain, Science Bulletin, 65, 765-774, doi:10.1016/j.scib.2020.02.006, 2020a.

Wang, Y., Gao, W., Wang, S., Song, T., Gong, Z., Ji, D., Wang, L., Liu, Z., Tang, G., Huo, Y., Tian, S., Li, J., Li, M., Yang, Y., Chu, B., Pet¨aj¨a, T., Kerminen, V.-M., He, H., Hao, J., Kulmala, M., Wang, Y., and Zhang, Y.: Contrasting trends of $PM_{2.5}$ and surface-ozone concentrations in China from 2013 to 2017, National Science Review, 7, 1331-1339, doi:10.1093/nsr/nwaa032, 2020b.

Wu, C., Liu, L., Wang, G., Zhang, S., Li, G., Lv, S., Li, J., Wang, F., Meng, J., and Zeng, Y.: Important contribution of N_2O_5 hydrolysis to the daytime nitrate in Xi'an, China during haze periods: Isotopic analysis and WRF-Chem model simulation, Environmental Pollution, 288, 117712, doi:10.1016/j.envpol.2021.117712, 2021.

Xie, Y., Wang, G., Wang, X., Chen, J., Chen, Y., Tang, G., Wang, L., Ge, S., Xue, G., Wang, Y., and Gao, J.: Nitrate-dominated $PM_{2.5}$ and elevation of particle pH observed in urban Beijing during the winter of 2017, Atmos. Chem. Phys., 20, 5019-5033, doi:10.5194/acp-20-5019-2020, 2020.

Xu, Q., Wang, S., Jiang, J., Bhattarai, N., Li, X., Chang, X., Qiu, X., Zheng, M., Hua, Y., and Hao, J.: Nitrate dominates the chemical composition of $PM_{2.5}$ during haze event in Beijing, China, Science of The Total Environment, 689, 1293-1303, doi:10.1016/j.scitotenv.2019.06.294, 2019a.

Xu, W., Sun, Y., Wang, Q., Zhao, J., Wang, J., Ge, X., Xie, C., Zhou, W., Du, W., Li, J., Fu, P., Wang, Z., Worsnop, D. R., and Coe, H.: Changes in Aerosol Chemistry From 2014 to 2016 in Winter in Beijing: Insights From High-Resolution Aerosol Mass Spectrometry, Journal of Geophysical Research: Atmospheres, 124, 1132-1147, doi:10.1029/2018JD029245, 2019b.

Xu, Z., Liu, M., Zhang, M., Song, Y., Wang, S., Zhang, L., Xu, T., Wang, T., Yan, C., Zhou, T., Sun, Y., Pan, Y., Hu, M., Zheng, M., and Zhu, T.: High efficiency of livestock ammonia emission controls in alleviating particulate nitrate during a severe winter haze episode in northern China, Atmos. Chem. Phys., 19, 5605-5613, doi:10.5194/acp-19-5605-2019, 2019c.

Xue, C., Zhang, C., Ye, C., Liu, P., Catoire, V., Krysztofiak, G., Chen, H., Ren, Y., Zhao, X., Wang, J., Zhang, F., Zhang, C., Zhang, J., An, J., Wang, T., Chen, J., Kleffmann, J., Mellouki, A., and Mu, Y.: HONO Budget and Its Role in Nitrate Formation in the Rural North China Plain, Environmental Science & Technology, 54, 11048-11057, doi:10.1021/acs.est.0c01832, 2020.

Xue, J., Yu, X., Yuan, Z., Griffith, S. M., Lau, A. K. H., Seinfeld, J. H., and Yu, J. Z.: Efficient control of atmospheric sulfate production based on three formation regimes, Nature Geoscience, 12, 977-982,

https://doi.org/10.5194/egusphere-2024-3044
Preprint. Discussion started: 30 October 2024

900 doi:10.1038/s41561-019-0485-5, 2019.

Yan, F., Gao, Y., Ma, M., Liu, C., Ji, X., Zhao, F., Yao, X., and Gao, H.: Revealing the modulation of boundary conditions and governing processes on ozone formation over northern China in June 2017, Environmental Pollution, 272, 115999, doi:10.1016/j.envpol.2020.115999, 2021.

Yang, J., Au, W. C., Law, H., Lam, C. H., and Nah, T.: Formation and evolution of brown carbon during 905 aqueous-phase nitrate-mediated photooxidation of guaiacol and 5-nitroguaiacol, Atmospheric Environment, 254, 118401, doi:10.1016/j.atmosenv.2021.118401, 2021.

Yang, J., Qu, Y., Chen, Y., Zhang, J., Liu, X., Niu, H., and An, J.: Dominant physical and chemical processes impacting nitrate in Shandong of the North China Plain during winter haze events, Science of The Total Environment, 912, 169065, doi:10.1016/j.scitotenv.2023.169065, 2024.

910 Ye, C., Zhou, X., Pu, D., Stutz, J., Festa, J., Spolaor, M., Tsai, C., Cantrell, C., Mauldin, R. L., Campos, T., Weinheimer, A., Hornbrook, R. S., Apel, E. C., Guenther, A., Kaser, L., Yuan, B., Karl, T., Haggerty, J., Hall, S., Ullmann, K., Smith, J. N., Ortega, J., and Knote, C.: Rapid cycling of reactive nitrogen in the marine boundary layer, Nature, 532, 489-491,doi:10.1038/nature17195, 2016.

Yu, F., Luo, G., Nair, A. A., Schwab, J. J., Sherman, J. P., and Zhang, Y.: Wintertime new particle 915 formation and its contribution to cloud condensation nuclei in the Northeastern United States, Atmos. Chem. Phys., 20, 2591-2601, doi:10.5194/acp-20-2591-2020, 2020.

Zang, H., Zhao, Y., Huo, J., Zhao, Q., Fu, Q., Duan, Y., Shao, J., Huang, C., An, J., Xue, L., Li, Z., Li, C., and Xiao, H.: High atmospheric oxidation capacity drives wintertime nitrate pollution in the eastern Yangtze River Delta of China, Atmos. Chem. Phys., 22, 4355-4374, doi:10.5194/acp-22-4355-2022, 920 2022.

Zhai, S., Jacob, D. J., Wang, X., Shen, L., Li, K., Zhang, Y., Gui, K., Zhao, T., and Liao, H.: Fine particulate matter ($PM_{2.5}$) trends in China, 2013–2018: separating contributions from anthropogenic emissions and meteorology, Atmos. Chem. Phys., 19, 11031-11041, doi:10.5194/acp-19-11031-2019, 2019.

925 Zhai, S., Jacob, D. J., Wang, X., Liu, Z., Wen, T., Shah, V., Li, K., Moch, J. M., Bates, K. H., Song, S., Shen, L., Zhang, Y., Luo, G., Yu, F., Sun, Y., Wang, L., Qi, M., Tao, J., Gui, K., Xu, H., Zhang, Q., Zhao, T., Wang, Y., Lee, H. C., Choi, H., and Liao, H.: Control of particulate nitrate air pollution in China, Nature Geoscience, 14, 389-395, doi:10.1038/s41561-021-00726-z, 2021.

https://doi.org/10.5194/egusphere-2024-3044
Preprint. Discussion started: 30 October 2024

Zhang, C., Liao, H., Li , K., Dai, H., and Gu, Z.: Numerical Simulation of Summertime OH Concentrations in China Since the Implementation of the Air Pollution Prevention and Control Action Plan, Chinese Journal of Atmospheric Sciences (in Chinese), 47, 713-724, doi:10.3878/j.issn.1006-9895.2112.21218, 2023a.

Zhang, Q., Zheng, Y., Tong, D., Shao, M., Wang, S., Zhang, Y., Xu, X., Wang, J., He, H., Liu, W., Ding, Y., Lei, Y., Li, J., Wang, Z., Zhang, X., Wang, Y., Cheng, J., Liu, Y., Shi, Q., Yan, L., Geng, G., Hong, C., Li, M., Liu, F., Zheng, B., Cao, J., Ding, A., Gao, J., Fu, Q., Huo, J., Liu, B., Liu, Z., Yang, F., He, K., and Hao, J.: Drivers of improved $PM_{2.5}$ air quality in China from 2013 to 2017, Proceedings of the National Academy of Sciences, 116, 24463-24469, doi:10.1073/pnas.1907956116, 2019.

Zhang, X., Tong, S., Jia, C., Zhang, W., Wang, Z., Tang, G., Hu, B., Liu, Z., Wang, L., Zhao, P., Pan, Y., and Ge, M.: Elucidating HONO formation mechanism and its essential contribution to OH during haze events, npj Climate and Atmospheric Science, 6, 55, doi:10.1038/s41612-023-00371-w, 2023b.

Zhang, Z., Jiang, Z., Guan, H., Liang, Y., Zheng, N., and Guo, W.: Isotopic Evidence for the High Contribution of Wintertime Photochemistry to Particulate Nitrate Formation in Northern China, Journal of Geophysical Research: Atmospheres, 126, e2021JD035324, doi:10.1029/2021JD035324, 2021.

Zhao, X., Zhao, X., Liu, P., Chen, D., Zhang, C., Xue, C., Liu, J., Xu, J., and Mu, Y.: Transport Pathways of Nitrate Formed from Nocturnal N_2O_5 Hydrolysis Aloft to the Ground Level in Winter North China Plain, Environmental Science & Technology, 57, 2715-2725, doi:10.1021/acs.est.3c00086, 2023.

Zhao, Z.-Y., Zhang, Y.-L., Lin, Y.-C., Song, W.-H., Yu, H.-R., Fan, M.-Y., Hong, Y.-H., Yang, X.-Y., Li, H.-Y., and Cao, F.: Continental Emissions Influence the Sources and Formation Mechanisms of Marine Nitrate Aerosols in Spring Over the Bohai Sea and Yellow Sea Inferred From Stable Isotopes, Journal of Geophysical Research: Atmospheres, 129, e2023JD040541, doi:10.1029/2023JD040541, 2024.

Zheng, B., Tong, D., Li, M., Liu, F., Hong, C., Geng, G., Li, H., Li, X., Peng, L., Qi, J., Yan, L., Zhang, Y., Zhao, H., Zheng, Y., He, K., and Zhang, Q.: Trends in China's anthropogenic emissions since 2010 as the consequence of clean air actions, Atmos. Chem. Phys., 18, 14095-14111, doi:10.5194/acp-18-14095-2018, 2018.

Zheng, G. J., Duan, F. K., Su, H., Ma, Y. L., Cheng, Y., Zheng, B., Zhang, Q., Huang, T., Kimoto, T., Chang, D., Pöschl, U., Cheng, Y. F., and He, K. B.: Exploring the severe winter haze in Beijing: the impact of synoptic weather, regional transport and heterogeneous reactions, Atmos. Chem. Phys., 15,

https://doi.org/10.5194/egusphere-2024-3044
Preprint. Discussion started: 30 October 2024

2969-2983, doi:10.5194/acp-15-2969-2015, 2015.

Zheng, H., Song, S., Sarwar, G., Gen, M., Wang, S., Ding, D., Chang, X., Zhang, S., Xing, J., Sun, Y., Ji, D., Chan, C. K., Gao, J., and McElroy, M. B.: Contribution of Particulate Nitrate Photolysis to Heterogeneous Sulfate Formation for Winter Haze in China, Environmental Science & Technology Letters, 7, 632-638, doi:10.1021/acs.estlett.0c00368, 2020.

Zhong, X., Shen, H., Zhao, M., Zhang, J., Sun, Y., Liu, Y., Zhang, Y., Shan, Y., Li, H., Mu, J., Yang, Y., Nie, Y., Tang, J., Dong, C., Wang, X., Zhu, Y., Guo, M., Wang, W., and Xue, L.: Nitrous acid budgets in the coastal atmosphere: potential daytime marine sources, Atmos. Chem. Phys., 23, 14761-14778, doi:10.5194/acp-23-14761-2023, 2023.

Zhou, W., Gao, M., He, Y., Wang, Q., Xie, C., Xu, W., Zhao, J., Du, W., Qiu, Y., Lei, L., Fu, P., Wang, Z., Worsnop, D. R., Zhang, Q., and Sun, Y.: Response of aerosol chemistry to clean air action in Beijing, China: Insights from two-year ACSM measurements and model simulations, Environmental Pollution, 255, 113345, doi:10.1016/j.envpol.2019.113345, 2019.

Zong, Z., Tan, Y., Wang, X., Tian, C., Li, J., Fang, Y., Chen, Y., Cui, S., and Zhang, G.: Dual-modelling-based source apportionment of NOx in five Chinese megacities: Providing the isotopic footprint from 2013 to 2014, Environment International, 137, 105592, doi:10.1016/j.envint.2020.105592, 2020.